Title: Formation, structure and climatic significance of blue rings and frost rings in high elevation bristlecone pine (*Pinus longaeva* D.K. Bailey)

Authors: Tardif[1], J.C., Salzer[2], M.W., Conciatori[1], F., Bunn[3], A.G., and Hughes[2], M.K.

Affiliations:

[1] Centre for Forest Interdisciplinary Research (C-FIR), University of Winnipeg, 515 Portage Avenue, Winnipeg, MB Canada R3B 29E

[2] Laboratory of Tree-Ring Research, The University of Arizona, 1215 E. Lowell St., Tucson, Arizona 85721, USA

[3] Department of Environmental Sciences, Western Washington University, Bellingham, WA, USA

[*] **Corresponding Author:** Jacques C. Tardif
Centre for Forest Interdisciplinary Research (C-FIR)
University of Winnipeg,
515 Portage Avenue
Winnipeg, Manitoba
R3B 2E9, Canada
Phone: 1-204-786-9475
Email: j.tardif@uwinnipeg.ca

Abstract: The study of anatomical irregularities in tree rings has recently gained momentum as a complement to traditional tree-ring measurements as they may provide information on extreme climatic events. Two anomalies, blue rings (BR) and frost rings (FR), were analyzed in bristlecone pine (*Pinus longaeva* D.K. Bailey) trees located along an elevation gradient in northeastern Nevada. These two subannual ring anomalies were systematically compiled for two periods; one centered on 536 CE (well-known for a volcanically-induced period of climatic cooling) and the other on 1965 CE (useful due to the availability of instrumental climate data). During the period 523-545 CE (n ≥10 trees), both BR and latewood FR (LWFR) were recorded abundantly in 532 and 536, as well as a BR cluster from 539-542 CE. Years when trees solely recorded a BR (without an accompanying LWFR) were more frequent in the earlier period than in the modern period (1954-2006 CE; n ≥10 trees) when both anomalies tended to co-occur. These results suggest a shorter growing season in the 536 period than in the 20th century. Modern BR/LWFR were most abundant in 1965 and 1978 CE. Both anomalies were mainly observed in the highest elevation trees and both were produced in years characterized by cooler than average temperatures throughout the growing season. Anatomically, BR and LWFR did not differ significantly in tracheid dimensions except that LWFR clearly showed damages associated with sub-freezing temperatures. The main feature distinguishing BR and LWFR from "normal" tree rings was a significant reduction in latewood secondary wall thickness. In *P. longaeva*, BR like pale latewood (light) rings, result from short and cool growing seasons which leads to reduced (or interrupted) lignification of tracheids. In species producing extremely narrow latewood like *P. longaeva* it may be difficult to macroscopically identify pale latewood years, thus rendering microscopic investigation of BR as a climate proxy useful in paleoclimatic research.

Keywords: North America, high elevation, tree rings, latewood tracheid, paleoclimatology, climate extremes, 536 and 1965 CE, dust veil, volcanic eruption, Holocene

1.0 Introduction:

1.1 Tree-Ring Anomalies and Climate

The study of tree-ring anomalies (anatomical irregularities), of their anatomical characteristics and of the environmental factors at their origin, in particular extreme climatic events, has recently regained attention in dendrochronology and paleoclimatology (Wimmer 2002; Schweingruber 2007; Bräuning *et al.* 2016). Such studies provide information on past environmental processes that occurred during the growing season of sets of trees (Tardif *et al.* 2011; Hadad *et al.* 2020 and references below). Comparisons can then be made along environmental gradients and across temporal scales to help inform questions regarding ecological and climatic processes. Tree-ring anomalies can also provide an exactly dated proxy record of climate events occurring at local, hemispheric and global scales. Anomalies, like frost rings (Glerum and Farrar 1966; LaMarche 1970; Hantemirov *et al.* 2004; Gurskaya and Shiyatov 2006; Waito *et al.* 2013; Gurskaya 2014; Montwé *et al.* 2018; Hadad *et al.* 2019; Barbosa *et al.* 2019; Hadad *et al.* 2020), false rings (Wimmer *et al.* 2000; Hoffer and Tardif 2009; De Micco *et al.* 2016) and pale latewood rings (also referred to as light rings; Brunstein 1995; Szeicz 1996; Gindl and Grabner 2000; Girardin *et al.* 2009; Tardif *et al.* 2011; Montwé *et al.* 2018) have long been studied from a wood anatomical perspective and for their climatic significance. More recently the study of white earlywood rings (Waito *et al.* 2013), dark rings (Novak *et al.* 2016) and blue rings (Piermattei *et al.* 2015) have broadened understanding of environmental forcing on tree-ring formation.

Frost damage to xylem tissue during the active growing season has been linked to the production of frost rings (FR). These rings are characterized by the presence of collapsed/crushed/abnormal tracheids with lateral expansion and displacement of the rays (Glerum and Farrar 1966; Schweingruber 2007). The position of a FR within a tree's annual ring can also provide information regarding the timing of frost events (LaMarche and Hirschboeck 1984; Gurskaya 2014; Barbosa *et al.* 2019). Frost-ring intensity varies according to the level of cambial activity at the time of the event and also with the temperature and duration of the frost. Latewood FR (LWFR) have been observed in high-elevation Great Basin bristlecone pine (*Pinus longaeva* D.K. Bailey) and in Rocky Mountain bristlecone pine (*Pinus aristata* Engelm.). These cold-damaged rings have been associated with volcanically-forced cooling events (LaMarche and Hirschboeck 1984; Brunstein 1996; Salzer and Hughes 2007). In contrast to LWFR, EWFR in bristlecone pine were reported to be scarce (LaMarche 1970; LaMarche and Hirschboeck 1984; Brunstein 1995).

Blue rings (BR) were first identified in European black pine (*Pinus nigra* Arnold) and were defined as tree rings showing the presence of "… a continuous layer of unlignified axial tracheids occurring either in the earlywood or in the latewood" (Piermattei *et al.* 2015). Blue rings were observed after double staining tree-ring thin transverse sections (15–20 µm) with Safranin and Astra blue dyes. Cell walls that did not sufficiently lignify during the growing season take on the blue color (Piermattei *et al.* 2015). Blue rings were also recently described in Scots pine (*Pinus sylvestris* L.) trees growing in Romania (Semeniuc *et al.* 2016) and Latvia

(Matisons *et al*. 2020), in lodgepole pine (*Pinus contorta* Dougl.) trees growing in western Canada (Montwé et al. 2018) and in *P. longaeva* trees growing in western United States (Hughes *et al.* 2016), again featuring the presence of under-lignified tracheids. The main hypothesis related to latewood BR formation calls for the observed lack of lignification in tracheids to be caused by low air temperature at the end of the growing season (Piermattei *et al.* 2015; Semeniuc *et al.* 2016). Similar climatic events are also believe to form pale latewood (light) rings (Szeicz 1996; Gindl and Grabner 2000; Gindl *et al.* 2000; Girardin *et al.* 2009; Tardif *et al.* 2011). In timberline spruce (*Picea abies* (L.) Karst.) light rings (LR) were shown to have latewood cells with reduced lignin content due to interference by cooler temperature towards the end of the growing season (Gindl and Grabner 2000; Grindl *et al.* 2000). A delayed growing season as well as cooler early and late growing seasons have also been stressed (Szeicz 1996; Girardin *et al.* 2009; Tardif *et al.* 2011). Interestingly, Brunstein (1995) mentioned that LR and LWFR often co-occurred in *P. aristata* trees. Hantemirov *et al.* (2004) also observed the co-occurrence of LR and FR in Siberian juniper (*Juniperus sibirica* Burgsd.) and in Siberian larch (*Larix sibirica* Ledeb.). Bräuning *et al.* (2016) suggested that the term BR may simply be another representation of LR using an alternative detection method. Montwé *et al.* (2018) implied that both BR and LR described essentially the same anomaly, i.e. tree rings with tracheids showing a lack of complete cell lignification. Further, Matisons *et al.* (2020) equated BR with early frost in late summer.

1.2 Tree Rings and Volcanic Eruptions in 536 and 1965 CE

In this paper, both BR and FR in *P. longaeva* were analyzed focussing on two periods centered on 536 and 1965 CE (hereafter all dates will refer to the Common Era unless otherwise

112 specified). The period centered on 536 is central to the Dark Ages Cold Period (410-775, Helama
113 *et al.* 2017) and to the recently described Late Antique Little Ice Age (536-660; Büntgen *et al.*
114 2016). Major volcanic eruption signatures identified in high-resolution ice-core records of
115 volcanic sulfur were reported during the mid-6th century in 536 and 540. This is thought to have
116 caused global low irradiance, climatic cooling and major societal impacts (Larsen *et al.* 2008;
117 Sigl *et al.* 2015; Büntgen *et al.* 2016; Helama *et al.* 2018; Newfield 2018). Toohey *et al.* (2016)
118 indicated that the combined impact of the 536 and 540 volcanic eruptions was unprecedented in
119 the last 1200 years leading to mean temperature anomalies of more than -2 °C in the Northern
120 Hemisphere. While uncertainties remain regarding the origin of these volcanic eruptions, the El
121 Chichón volcano (Mexico; Nooren *et al.* 2017) and the Ilopango volcano (El Salvador; Dull et
122 *al*. 2019) were identified as the potential source for the 540 tropical eruption. The societal
123 impacts of the 536 and 540 eruptions are a subject of ongoing debate. Some emerging criticism
124 has focused on environmental determinism and potentially too large a role attributed to the
125 volcanic eruptions when assessing the cultural volatility of the 6th century (Haldon 2016;
126 Moreland 2018).

127

128 Tree-ring indicators suggest the existence of global-scale temperature anomalies centered on 536
129 (see review by Newfield 2018) as indicated by the formation of FR in trees growing in high-
130 altitude regions in northern hemisphere. Helama *et al. (*2019) recently reported a FR dated to 536
131 in the latewood of subfossil *P. sylvestris* trees from Finish Lapland. Using stable carbon isotopes
132 to model solar radiation, Helama *et al.* (2018) reported an irradiance decline for 536 and 541–
133 544 attributing these negative departures to volcanic dust veil. At high-latitude sites from
134 southern Siberia, Churakova (Sidorova) *et al.* (2014) reported FR dated to 536 in the latewood of

larch trees. The major cooling around 536 was also supported by measurements of ring width, cell-wall thickness, and stable carbon ($\delta^{13}C/\ \delta^{12}C$) and oxygen ($\delta^{18}O/\ \delta^{16}O$) isotope ratios in cellulose (Churakova (Sidorova) *et al.* 2014). In 536, the observed reduction in ring width and cell wall thickness as well as the strong decline in $\delta^{13}C$ and $\delta^{18}O$ values all supported the existence of a major cooling of air temperature during the growing season. In the same year, FR were also observed in the mid-earlywood of Siberian pine (*Pinus sibirica* Du Tour) trees growing at the Mongolia timberline (D'Arrigo *et al.* 2001). At upper forest border bristlecone pine sites in the western United States, LWFR have also been reported in 536 in numerous trees (Brunstein 1995; 1996; Salzer and Hughes 2007).

Many of the FR years identified by LaMarche and Hirschboeck (1984), Hallman (2001) and Salzer and Hughes (2007), including 536 and 1965, have been linked to volcanic eruptions. Brunstein (1995) also mentioned that LR and FR co-occurred in *P. aristata* trees in these two years. The 1965 LWFR is thought to be associated with the Mount Agung eruption (Indonesia) in 1963-64 (LaMarche and Hirschboeck 1984). LaMarche (1970) associated this anomaly with a delayed and cool growing season with sub-freezing temperature at upper treeline elevations in mid-September in Nevada. In this case, cooler than average summers delayed both the onset and the completion of cambial activity rendering trees more susceptive to end of season damaging frosts (LaMarche and Hirschboeck 1984). Modern (1900-1992) LWFR in *P. longaeva*, similar in appearance to those identified in 536, have also been linked to cold growing seasons in Colorado, with record subfreezing temperature in early to mid-September in Colorado as well as severe outbreaks of cold air across the western United States in 1965 from June to September (1.5-2.0 °C cooler than normal; Brunstein 1996). The seasonal timing of the formation of LWFR

158 and BR in *P. longaeva* has also been recently reinforced by xylogenesis studies of *P. longaeva*
159 trees growing in the Great Basin (3355 m a.s.l). This work indicates that the onset of xylem
160 formation generally started in early June (mean air temperature reaching ~7 °C) with tracheid
161 maturation being completed by mid-September (Ziaco *et al*. 2016b).

162

163 In dendroclimatology, linking tree-ring features to large-scale circulation has a long tradition. In
164 their review, Hirschboeck *et al*. (1996) stated that both dendroclimatology and synoptic
165 climatology have had a parallel and interconnected development. Synoptic dendroclimatology
166 aims at connecting "extreme" climate events recorded in tree rings to large-scale circulation by
167 using techniques such as indexing, correlation fields and composite maps (Hirschboeck *et al*.
168 1996). Composite maps were used by Stahle (1990) to summarize the conditions involved in the
169 development of weather systems leading to false springs and EWFR formation in post oak
170 (*Quercus stellata* Wangenh.) trees growing in the southern Great Plains of the United States.
171 Early growth resumption (false spring) was found to be a major component associated with the
172 formation of EWFR and false springs were often observed during strong La Niña conditions.
173 Hadad *et al*. (2019) also reported that EWFR in chihuén (*Araucaria araucana* (Molina) K. Koch)
174 trees from Argentina were more abundant in La Niña events which correspond to earlier spring
175 in South America. Composite maps provided evidences that sub-freezing events in Argentina
176 were associated with an anomalous trough crossing the region at 500 hPa in NW–SE direction.
177 Hadad *et al*. (2020) also showed that earlywood FR in black spruce (*Picea mariana* (Mill.)
178 B.S.P.) trees growing in interior North America were associated with early spring which
179 corresponded to the prevalence in April of a high-pressure system over central Canada. The

authors also discussed the influence of the El Niño-Southern Oscillation (ENSO) in being related to the occurrence of false springs in interior North America.

Hirschboeck *et al*. (1996) analyzed the atmospheric circulation associated with the 1965 LWFR in subalpine bristlecone pine in several localities from the western United States. The authors found that, at both monthly and daily scales, the 1965 LWFR was linked to the development of a strong ridge over the Gulf of Alaska leading to a deep trough located over the western United States and conveying Artic air masses. In the Colorado Rockies, composite maps indicated that both earlywood and latewood FR in *P. aristata* occurred during amplified mid- to high- latitude atmospheric circulation regimes resulting in cold surface air temperatures penetrating into the westcentral United States (Barbosa et al. 2019). Tardif *et al*. (2011) established that LR formation in jack pine trees growing in central Canada corresponded to cool summer temperature anomalies across wide areas of interior North America ranging as far as from Minnesota, United Stated, to the Baffin Island, Canada. Persistent positive height anomalies (ridges) over the Gulf of Alaska and negative height anomalies (troughs) east of the Hudson Bay, as revealed by 500-hPa geopotential heights composite maps, were associated with the LR formation. Hirschboeck *et al*. (1996) concluded that FR, despite being linked to short-term events (sub-freezing temperature), also contained climate information at a longer time scale making them an excellent proxy from which to evaluate anomalous circulation patterns. Blue rings like FR and LR are also likely linked to specific large-scale components of atmospheric circulation.

1.3 Objectives

The objectives of this study were i) to quantify both BR and LWFR in high-elevation *P. longaeva* trees from a wood anatomy perspective, ii) to discuss their presence in relation to climate and atmospheric circulation and iii) to assess their co-occurrence along an elevation gradient in the two time periods discussed above. One overall goal was to assess if threshold temperatures or particular climate conditions can be associated with BR and FR formation in the second-half of the 20th century so as to provide an analogue for their past occurrence. This research also contributes to discussion surrounding what has been referred to as the fine-scale spatial sensitivity in tree-ring climate response near the upper treeline (Bunn *et al.* 2011; Salzer *et al.* 2013; Salzer *et al.* 2014; Tran *et al.* 2017; Bunn *et al.* 2018).

2.0 Methods:

2.1 Study Area

The study area is Pearl Peak at the southern end of the Ruby Mountain Range (Fig. 1). It is located in northeastern Nevada (40.235 N. Lat., 115.542 W. Long.) within the Great Basin physiographic section of the Basin and Range Province of North America. Three tree-ring sites from Pearl Peak were used (PPL, 2996-3086 m; PPU, 3094-3221 m; and PRL, 3074-3291 m). These can be considered separate groves of trees or distinct areas within the upper treeline zone of Pearl Peak. See Salzer and Hughes (2007), Salzer *et al.* (2009), Salzer *et al.* (2013) and Bruening (2016) for further information regarding research that used this study location. These three sites were used because initial examinations of specimens from Pearl Peak revealed the existence of many FR in the trees from the upper treeline zone. For the 536 period

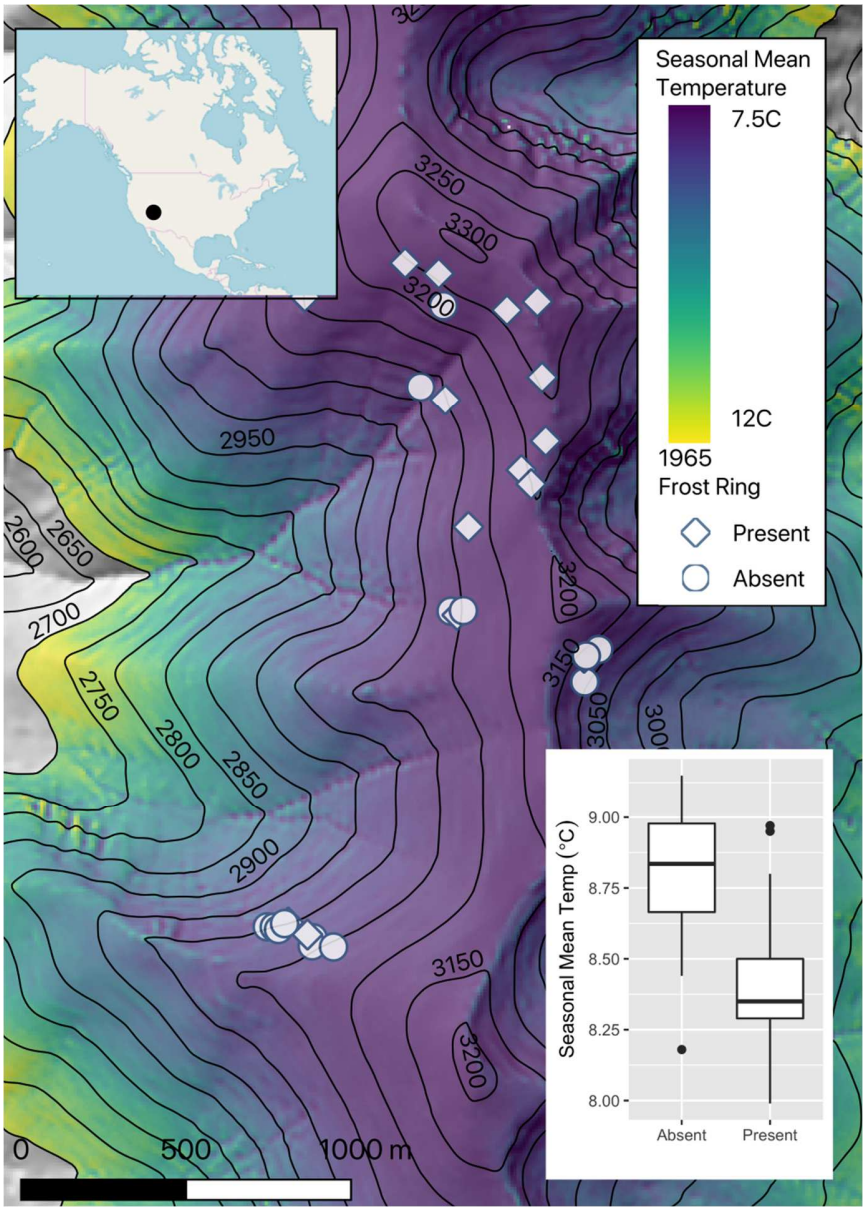

224

225 **Fig. 1:** Map of the study area. Upper left inset shows position of study area within North
226 America (black circle). Topographical map indicates location of *Pinus longaeva* trees recording
227 a latewood frost ring in 1965 in relation to derived topoclimate seasonal mean temperature
228 (upper right inset; see section 2.4.2 for details). The lower right inset indicates mean temperature
229 differences between tree locations for those recording the 1965 frost ring and those that did not.

all the samples that were available were used for that temporal interval and for which we were able to effectively cut a thin section for BR analysis. For the 1965 period the same constraint applied; all the living tree core samples along the elevational gradient were used and for which thin sectioning could be done without destroying the core.

2.2 Sample Collection

The tree-ring samples used in this study were collected over a twelve-year period from 2003 to 2014 as part of an ongoing research effort that use*s P. longaeva* as a paleoclimate proxy record (Salzer and Hughes 2007; Salzer *et al.* 2009, 2013; Tran *et al.* 2017, Bunn *et al.* 2018). Core samples from both living *P. longaeva* trees and from remnant wood pieces were used as well as small, hand-sawn samples from remnants. The living tree core samples used in the analyses of 1965 anomalies were roughly distributed along an elevation gradient (Fig. 1). For the 536 period, the 12 *P. longaeva* trees used were more evenly distributed elevationally, growing at a mean elevation of 3225 (±47 m asl). They had an average minimum age of 1150 (± 619 years). The 31 trees covering 1965 were growing at a lower elevation, 3126 (±92 m asl) and were younger, with an average minimum age of 554 (± 336 years).

2.3 Tree-Ring Anatomy and Image Analysis

Wood anatomical slides were produced from dried *P. longaeva* cores and cross-sections using a sledge microtome (AO Spencer N0. 860). Continuous thin sections were obtained for each

sample either corresponding to the period centered on 536 or 1965. In total, 12 (536) and 31 (1965) tree samples were thin-sectioned. All thin sections were prepared following standard methods (Gärtner *et al.* 2015; Tardif and Conciatori 2015). Prior to thin-sectioning, core samples were softened by applying water with a brush and approximately 16-18 µm thin sections were produced after applying a starch-based non-Newtonian fluid (Schneider and Gärtner 2013) and a water soluble glue (Mowiol 4-88 polyvinyl alcohol powder; Gärtner *et al.* 2015). A double-staining procedure (mixture of 1g safranin and 0.5 g of Astra blue each in 100 ml of distilled water and 2 ml of acetic acid) was applied. The thin sections were soaked in the mixture for a 3-5 min treatment and then rinsed with distilled water to remove excess dye. The sections were next placed in successive ethanol baths (50%, 75, 95% and 99.5%) for 1-2 min and then placed in clearing solvent (Safeclear II) for 1-2 min to clear them of remaining impurities prior to permanently mounting on standard microscope slides. After the anatomical slides were dried, they were visually scanned under a microscope to determine the occurrence of both BR and FR along the exactly annually dated tree-ring sequence (Fig. 2) and the BR and FR data were compiled.

Wood anatomy parameters were generated using image analysis of the 536 and 1965 tree rings. Twelve samples were analyzed for year 536 and 27 samples for year 1965 (four were dropped because of poor condition). The procedures used to measure tracheid dimensions were similar to those described in Waito *et al.* (2013). The prepared surfaces were photographed with a Nikon DS-FI1 digital camera connected to a Nikon Eclipse 200 microscope to generate color images at a 20x magnification and a resolution of 2560 x 1920 pixels. A Nikon blue microscope filter was used to increase the contrast between tracheid walls and the lumen. Adobe Photoshop Elements

(Ver 14.1) was used to merge images when necessary. Each image was then analyzed using software program WinCELL Pro V 2016c (Régent Instruments Inc. Canada). Correction of images, if needed, mainly involved increasing contrast between the tracheid lumen and cell wall boundaries and visually repairing damage to the tracheid cell walls that resulted from thin sectioning. Despite using a non-Newtonian fluid and a water soluble glue during thin section preparation, sectioning BR and LWFR with a microtome may be challenging due to the presence of under-lignified tracheids. Numerous slides for each sample were thus produced.

For each image, tracheid dimensions were measured along three radial files selected from the upper, middle, and lower portion of the image. The main criterion in selecting the three radial files was that they have minimal artefacts from slide preparation. Tracheids measured along the radial files were divided into an earlywood (EW) and latewood (LW) component using the average cell wall/lumen ratio >0.25. This tracheid classification (Mork's definition) however does not consider the wide variability in tree-ring structure associated with the study of tree-ring anomalies (Park *et al.* 2006) and a manual correction was applied when appropriate. In addition, each tracheid was also visually classified as being a BR or a LWFR tracheid. The tracheid features that were measured included number of tracheids (NT), lumen area [LA], radial lumen diameter [LD], average cell wall thickness [CWT; calculated as half the shared cell wall with the tracheid preceding and that following the tracheid being measured along the radial file] and the wall-to-tracheid ratio [WTR; calculated as CWT/LD]. This resulted in five anatomical parameters for the earlywood (EW), the latewood (LW) and for tracheid classified as BR and FR. The proportion of earlywood (EW%), latewood (LW%), blue ring (BR%) and frost ring

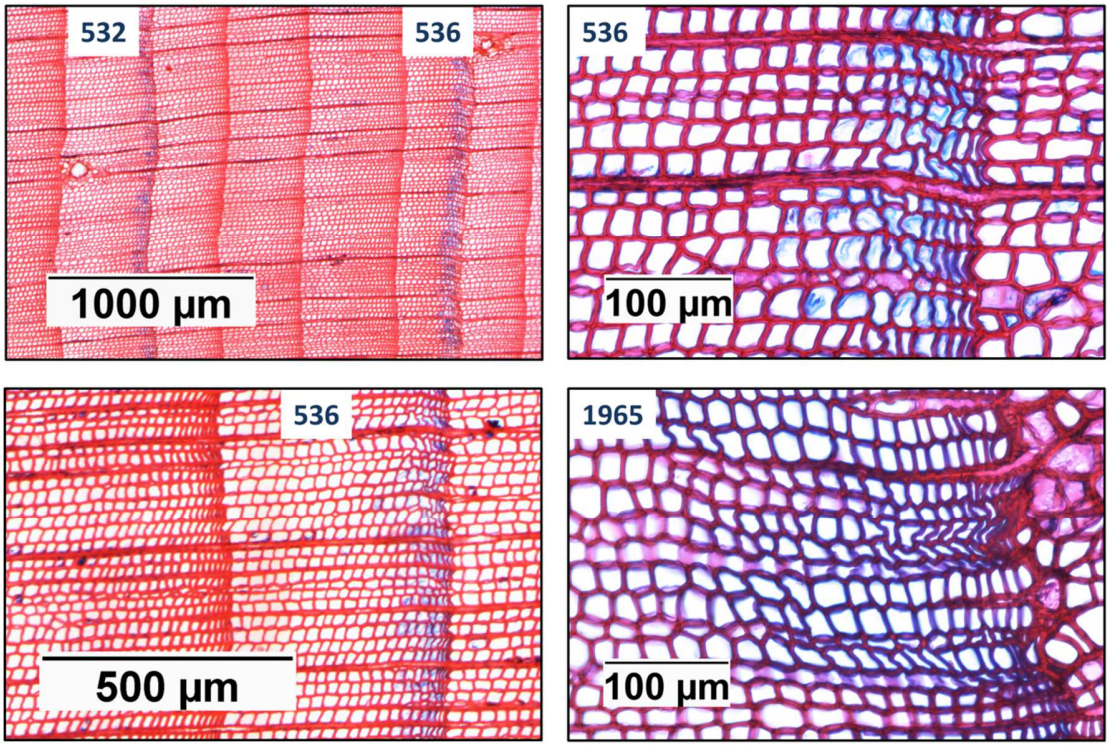

Fig. 2: *Pinus longaeva* samples showing both blue rings and frost rings in years 532, 536 or 1965 CE. All pictures come from different trees except that of the bottom left and upper right which came from the same tree and were respectively taken using a Nikon dissecting microscope SMZ1000 and a Nikon compound microscope Eclipse E200.

(FR%) tracheids was also calculated. For each sample, the average of the three radial files was calculated resulting in a total 24 anatomical parameters for each of the 536 (12 trees) and 1965 (27 trees) tree rings.

2.4 Statistical Analyses

2.4.1 Tree-Ring Anomalies and Climate

To evaluate the association between the frequency of tree-ring anomalies (BR and FR) and synoptic circulation, composite maps were made using the Climate Explorer facility (http://climexp.knmi.nl/; Trouet and van Oldenborgh 2013) of the Royal Netherlands Meteorological Institute (KNMI). Composite maps are particularly useful when derived from non-continuous, event-based time series (Hirschboeck *et al.* 1996; Trouet and van Oldenborgh 2013). Composite maps were derived using the NOAA-CIRES-DOE Twentieth Century Reanalysis (V3) monthly geopotential heights (HGT, in mgp) at 500 hPa level and in a global regular 1.0° × 1.0° latitude-longitude grid was used (Slivinski et al. 2019; NOAA/OAR/ESRL PSL, Boulder, Colorado, USA, https://psl.noaa.gov/). The objective was to identify and to compare dominant synoptic-scale circulation patterns associated with BR and FR formed during the period centered on 1965. The analyses were conducted over the period 1954-2006 which corresponded to the period when a minimum of ten trees were included in the tree-ring anomaly chronologies. To calculate the association with "local" climate, mean of monthly minimum and maximum temperature and total precipitation data were obtained for the grid pertaining to Pearl Peak (40.235 N. Lat. and 115.542 W. Long; Spatial resolution 4km, PRISM Climate Group, Oregon State University, http://prism.oregonstate.edu, created 18 Oct. 2019). All correlation

analyses between frequency of tree-ring anomalies (BR and both earlywood and latewood FR) and gridded climate data were done using Spearman's rho correlation due to the non-normal distribution of the 1954-2006 tree-ring anomalies. To complement the correlation analyses, we also tested for differences in mean monthly temperatures using the non-parametric Mann-Whitney U tests.

Because there are no long-term weather stations for the study area, we used atmospheric air temperatures at 500 mb height from the NOAA-CIRES-DOE 20CR V3 (Slivinski et al. 2019) from 1836 to 2015 to put BR and LWFR formations into a longer-term context. To better approximate temperature experienced by the trees we used daily interpolated surface temperature data PRISM (Daly *et al.* 2008) from 1982 to 2015 to adjust the NOAA-CIRES-DOE 20CR V3 data. Because these two data sets covary strongly, we modeled the surface temperature from PRISM using the reanalysis data to create a surface temperature from 1836 to 2015. We used a generalised least squares of the form $y_t = \beta_0 + \beta_1 x_t + \varepsilon_t$ where t is the time in days, y is the PRISM data, x is the NOAA-CIRES-DOE 20CR V3 data, β_0 and β_1 are coefficients and ε are autocorrelated residuals following an ARMA (1,2) process. This model had an R^2 of 0.83. Extending the surface temperature in this way allows us to put the years with abundant LWFR and BR into a longer-term context.

2.4.2 Tree-Ring Anomalies and Environmental Features

The environmental and climate setting between trees recording BR only, LWFR only and both BR/LWFR (recording trees) as compared to co-located trees without these anomalies (non-

recording trees) was examined using non-parametric Mann-Whitney U tests. First, we tested for differences in tree elevation in 536 (n=12), 1965 (n=31) and 1978 (n=29). In addition, topoclimate variables were derived for each tree location. Given that topography affects local climate at scales relevant to tree-ring formation (e.g. see Bunn et al. 2011), we tested to see if trees growing in cooler topographic locations might be more susceptible to record anatomical growth anomalies driven by colder temperatures as compared to trees in surrounding areas.

At Pearl Peak, Bruening (2016) and Bruening *et al.* (2017, 2018) used 50 temperature sensors arrayed across topographic gradients to model monthly temperature anomalies with topography ("topoclimate") at a 10-m horizontal resolution. Those data, and data from other Great Basin treeline sites, showed that topography attenuates maximum and minimum air temperatures beyond the expectations derived from elevational-lapse rates. In particular, Bruening *et al.* (2017) found that temperatures during the growing season vary according to topographic setting several times more than predicted by the dry adiabatic lapse rate. These observations have helped to explain variations in the position of the alpine treeline on the landscape (Bruening *et al.* 2017, 2018) as well as the growth response of individual trees (Tran *et al.* 2017; Bunn *et al.* 2018). We used four topoclimate variables developed by Bruening et al. (2017, 2018) to assess if BR and LWFR were recorded in trees in colder topoclimate settings than generally found even at the alpine treeline ecotone. These variables were mean temperatures in May and in September (respectively start and end of growing season), the length of growing season in days (LGS) defined as the sum of days with daily mean temperature above 0.9 °C, and the seasonal mean temperature in °C (SMT) (Körner 2012). SMT was defined as average of the daily mean temperatures for the days included in the LGS. These topoclimatic variables were calculated

following Bruening (2016), Bruening *et al*. (2017), and Tran *et al*. (2017) for each tree location, provided a way of integrating the deviation in temperature that a given tree experiences over the growing season.

2.4.3 Tree-Ring Anatomy of Blue and Latewood Frost Rings

To determine if the anatomical features in tree rings (EW and LW) differed significantly between recording (BR only, LWFR only and both BR/LWFR) and non-recording trees the non-parametric Kruskall-Wallis one-way analysis of variance was used. The Dunn-Bonferroni post-hoc method was performed following a significant Kruskal-Wallis test. Both year 536 (n=12) and 1965 (n=27) were pooled in this analysis. Additionally, to determine if BR tracheid features differed from LWFR ones, the Mann-Whitney U Test was performed.

Standardized tracheidograms were also produced to compare yearly tree-ring anatomical profiles (Vaganov 1990; Gindl 1999; Vaganov *et al.* 2006; Ziaco *et al.* 2014ab). Tracheidograms represent measurement profiles of tracheid dimensions across tree rings. Standardization allows for structural comparison of rings with a different number of cells (Vaganov *et al.* 2006). Yearly anatomical features (LA, LD, CWT and WTr) were computed using the "tgram" package (DeSoto *et al.* 2011; available from CRAN; https://cran.r-project.org) in R (R Core Team 2013). The tracheidograms for year 536 and 1965 were standardized to 20 cells which closely matched the average number of tracheids observed in the 1965 samples. This analysis allowed comparisons of tracheid dimensions for the year 536 and 1965 and of tree rings recording and not recording BR and FR. All standardized tracheidograms (536: n=36 radii pertaining to 12

trees and 1965: n=81 radii pertaining to 27 trees) were averaged to produce mean tracheidograms.

3.0 Results:

3.1 Blue Rings and Frost Rings: Their Frequency and Climatic Connection

In the mid-6th century both BR and LWFR were abundant in 532 and 536 and to a lesser extent in 574 and 525 (Fig. 3a). We also observed a cluster of BR from 539 to 542 with a maximum observed in 540. Few EWFR were observed and years with solely a BR being recorded were more abundant than for the second half of the 20th century (Fig. 3b). In the latter period, both BR and LWFR were recorded in high abundance in 1965 and 1978 and to a lesser extent in 1982. Earlywood FR never reached the same abundance as LWFR and were not synchronized with BR. In contrast, LWFR years and BR were synchronized; BR were typically observed in LWFR years.

Data from individual trees (not presented) indicated that, within a tree, LWFR were almost always associated with a BR, whereas tree rings showing only a BR or only a LWFR were less common. At the tree level and specifically looking at years 536 and 1965, of the recorder trees (10/12 and 18/27 respectively), most trees that recorded a BR also produced a LWFR (6/10, 12/18 respectively); few trees recorded solely a BR (3/10, 4/18 respectively) or a LWFR (1/10, 2/18 respectively). Chi-square testing for 1965 indicated that BR and LWFR were not independent and trees with BR recorded more LWFR than expected by chance (Pearson Chi-Square value= 811.519, p=0.001, n=31).

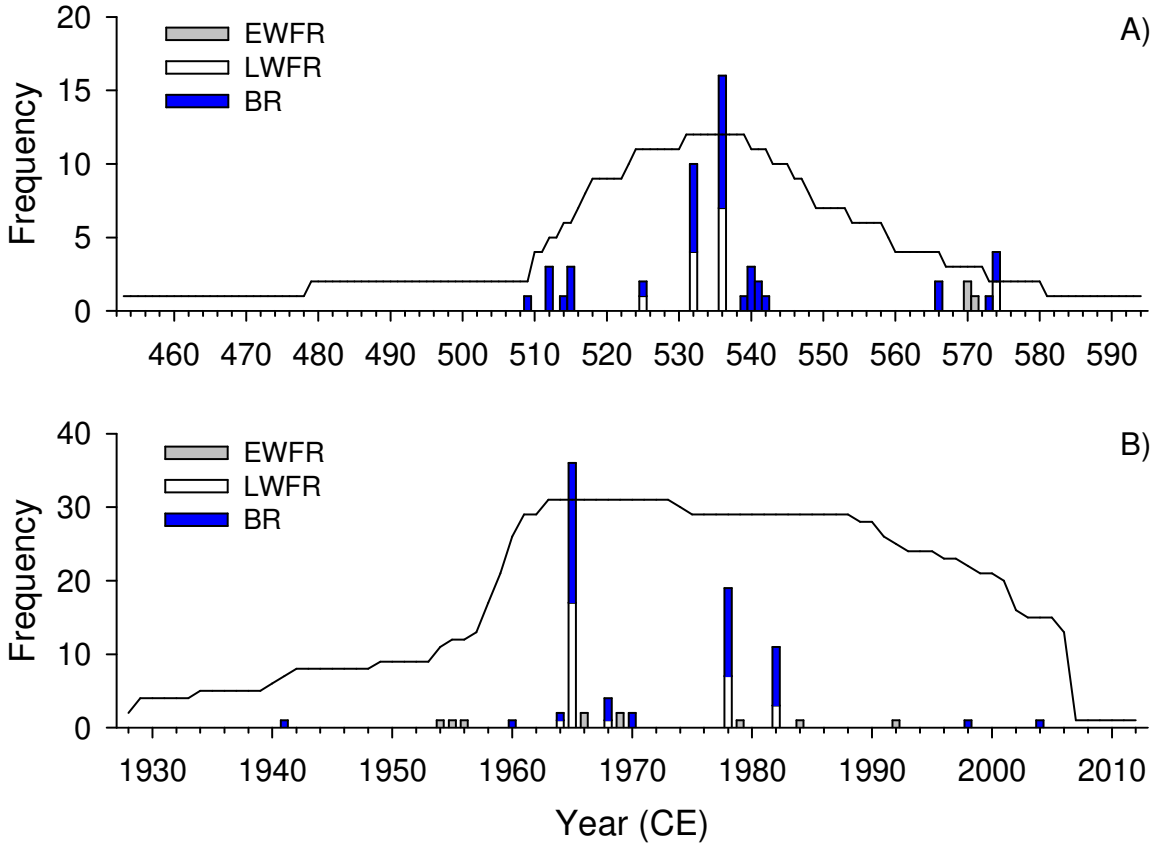

Fig. 3: Distribution of earlywood frost rings (EWFR), latewood frost rings (LWFR) and blue rings (BR) in *Pinus longaeva* trees within the 536 (A) and 1965 (B) CE periods. The number of samples is indicated by the solid line.

428 Correlating the portion of the chronologies pertaining to a minimum of 10 trees (1954-2006; Fig.
429 3b) with PRISM gridded climate data further supported the similarities between BR and LWFR
430 in contrast to EWFR (Fig. 4). Earlywood FR were negatively correlated to March precipitations
431 and positively to May maximum temperatures (Fig. 4). In contrast, both LWFR and BR were
432 found to be more frequent in years characterized by cooler minimum temperature in late spring
433 months (May and May-June; Fig. 4a). Blue ring and LWFR were also found to be more frequent
434 in years when maximum temperatures were cooler in the late growing season (August-
435 September) as well as during the entire growing season (Fig. 4b). Compared to BR, LWFR had
436 slightly stronger negative correlation with minimum temperatures. The Mann-Whitney U test
437 confirmed that the mean of May maximum temperatures was significantly warmer (by 2 °C) in
438 years forming EWFR (Suppl. Tables 1 and 2). In contrast, years with LWFR and BR recorded
439 significantly cooler minimum temperatures in May (1.5 and 1.4 °C respectively) with LWFR
440 years also recording significantly cooler minimum temperatures throughout the growing season.
441 Years with LWFR and BR also recorded significantly cooler maximum temperatures during the
442 growing season and in particular in the late portion of the growing season (Suppl. Tables 1 and
443 2). Further both the modeled surface daily temperature data for 1965, 1978 and 1982 (Fig. 5) and
444 the 500 mb daily temperature data (not presented) clearly indicated that in these three years
445 much of May, June and September fell below the long-term temperature average. Major sub-
446 freezing temperature departures were also observed in September (Fig. 5); these presumably
447 being the source of the frost damages at ground level.

448

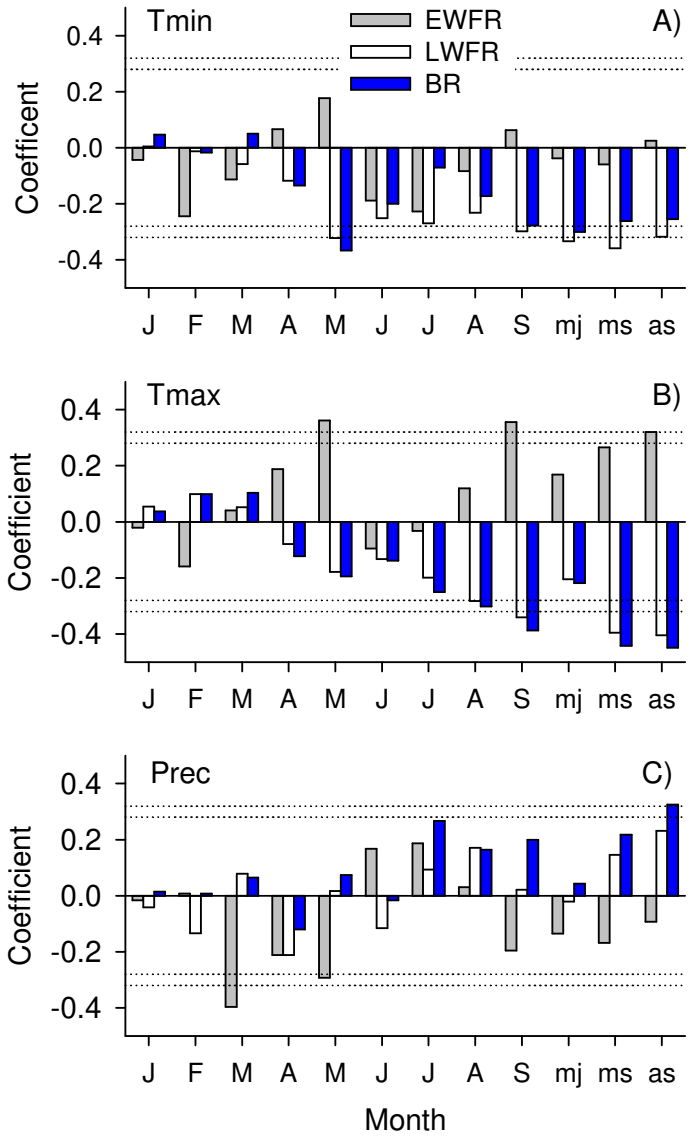

449

450 Fig. 4: Spearman rank correlation coefficients between earlywood frost rings (EWFR), latewood
451 frost rings (LWFR), blue rings (BR) chronologies and PRISM climate variables for the period
452 1954-2006. The dotted lines indicate significant correlation at $p<0.05$ and $p<0.01$. Capital letters
453 indicate months from January to September. mj: May and June average, ms: May to September
454 average and as: August and September average.

455

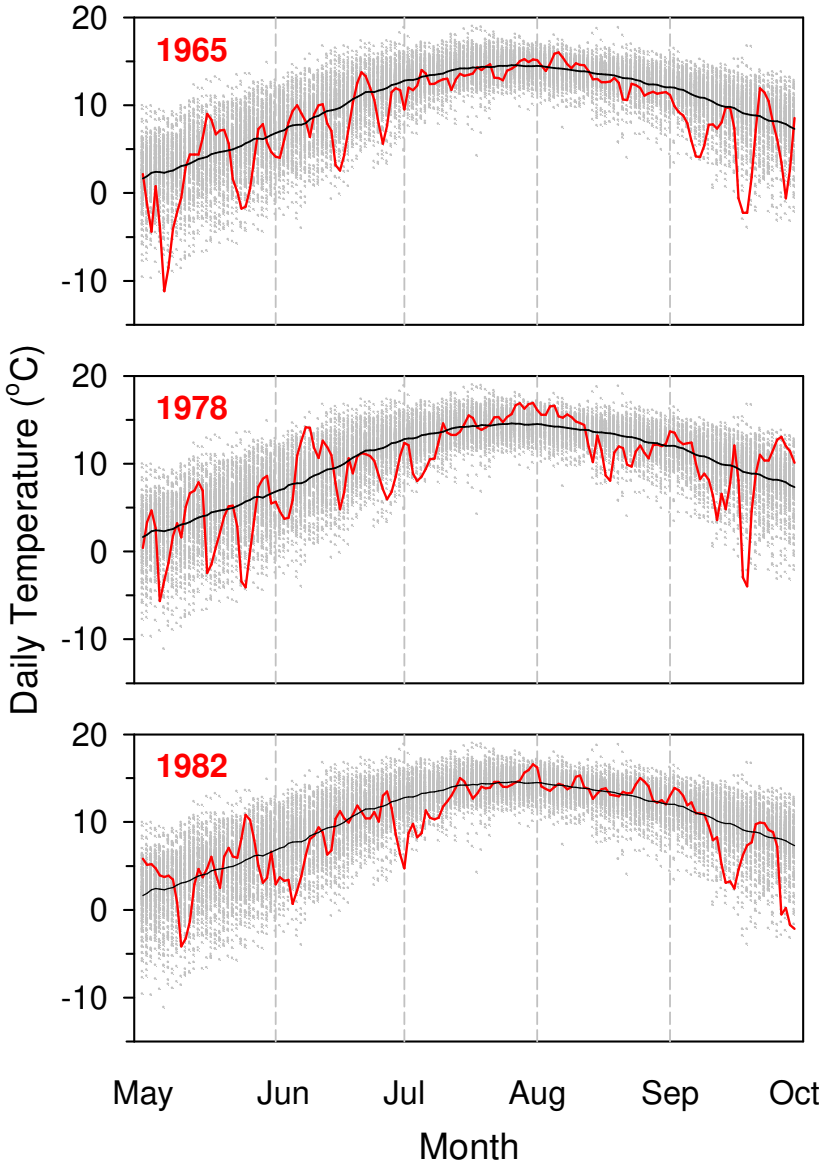

Fig. 5: Modeled surface daily temperatures from May 1st 1836 to September 30th 2015 (see section 2.4.1 for details). The black line is the daily mean for the entire period and the red lines indicate the years 1965, 1978 and 1982 (top to bottom). Note the severe September freezing episodes in 1965 and 1978.

462

463 At the hemispheric scale, the synoptic signal associated with EWFR was coherent with the
464 Spearman's rank correlation analyses and composite maps indicated that in EWFR years a high
465 ceiling (Great Basin High) in May prevailed over the study area (Fig. 6). The signal associated
466 with both BR and LWFR anomalies was coherent over a large portion of North America with
467 composite maps showing negative that both BR and LWFR were more common during years
468 when the growing season was characterized by a low pressure system (Great Basin Low)
469 persisting from May to September (Fig. 6). These results indicate that during BR (LWFR) years,
470 mean growing season temperatures were cooler than in non-recording years with significant
471 intrusions of cold air masses over the western portion of the United States. In the month of
472 September, the deep trough over the study area was particularly noticeable in BR years.
473 Inversely, EWFR may be more frequent in years characterized by warm Mays and an early
474 reactivation of cambial activity.

475

476 **3.2 Blue Ring, Latewood Frost Ring, Elevation and Topoclimate**

477 In order to account for BR and LWFR formation in *P. longaeva* trees, we tested for significant
478 differences between tree locations both in elevation and in topoclimatic features using years
479 when BR and LWFR were observed in a large number of trees i.e., 536, 1965 and 1978 (Figs. 1
480 and 3). The results indicated that elevation was most often discriminating among trees recording
481 or not recording a given anomaly (Table 1). In 1965 and 1978, a difference of about 100m was
482 observed between recorder and non-recorder trees. This difference in elevation reflects

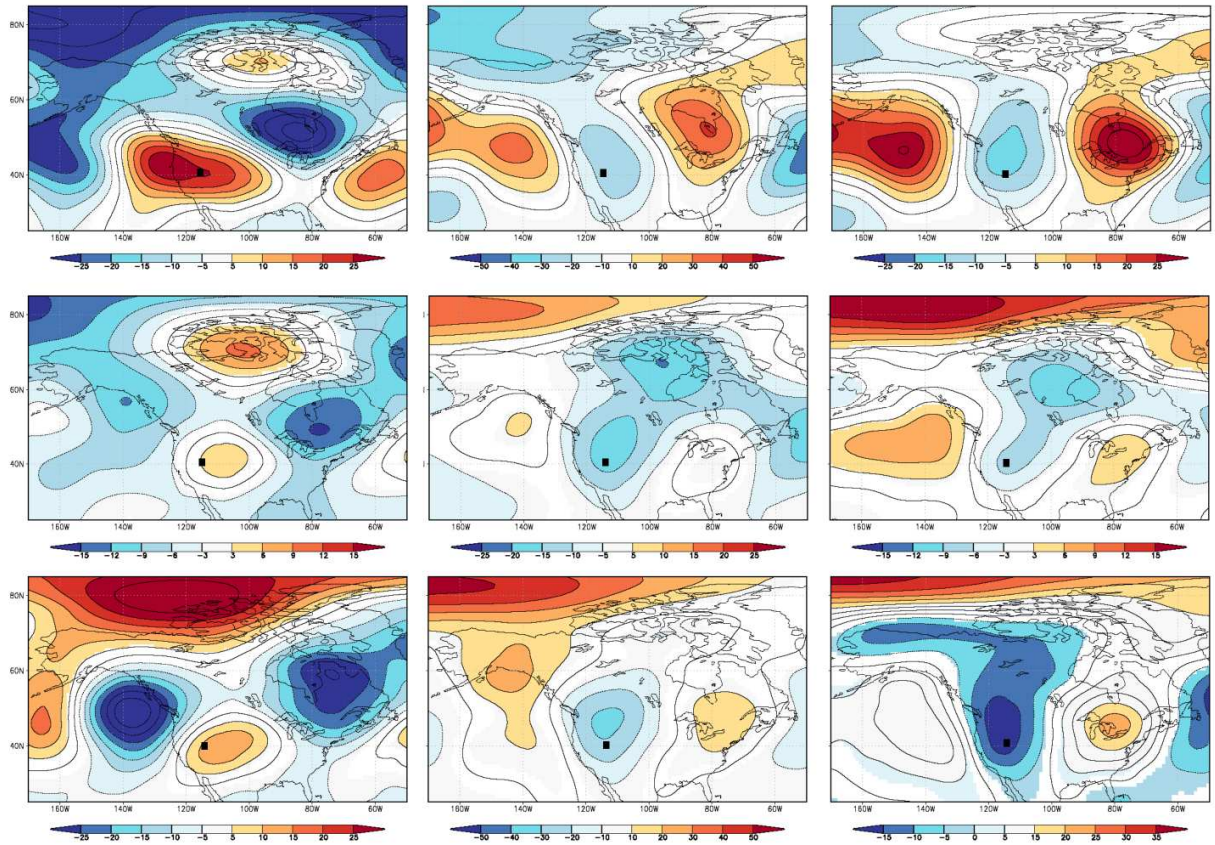

Fig. 6: Composite maps derived for years showing earlywood frost ring (left panel), latewood frost rings (middle panel) and blue ring (right panel) chronologies. The maps represent gridded monthly geopotential heights at 500 hPa level from NOAA-CIRES-DOE Twentieth Century Reanalysis (V3; NOAA/OAR/ESRL PSL, Boulder, Colorado, USA, https://psl.noaa.gov/) for May (upper), May to September (middle) and September (lower). The period of analysis is 1954-2006. The black square indicates position of the study area. The maps were created using the Royal Netherlands Meteorological Institute (KNMI) Climate Explorer.

Table 1: Mann-Whitney U test indicating significant differences in topographic (Elev: elevation) and topoclimatic (SMT: seasonal mean temperature; LGS: length of growing season in days) variables between trees not recording and recording a tree-ring anomaly (blue ring, frost ring and both) in years 536, 1965 and 1978. The mean and standard deviations are indicated. Note that the number of observations per group varies for each year analyzed. Bold number in shaded grey box indicates significant differences at $p<0.05$.

Year	Variables	NoBR	BR	Pvalue	NoLWFR	LWFR	Pvalue	NoBR-LWFR	BR-LWFR	Pvalue
536	N	3	9	----	5	7	----	6	6	----
	Elev.	3213 ±12	3230 ±54	0.482	3203 ±25	3242 ±54	0.073	32bb07 ±24	3244 ±59	0.065
	SMT[1]	8.4 ±0.1	8.1 ±0.2	0.100	8.3 ±0.1	8.1 ±0.2	0.073	8.3 ±0.1	8.1 ±0.2	**0.026**
	LGS[1]	148.3 ±1.2	146.9 ±5.3	0.482	148.6 ±2.6	146.3 ±5.7	0.106	148.7 ±2.3	145.8 ±6.1	0.065
	TmeanMay[1]	0.03 ±0.1	-0.23 ±1.0	0.482	0.04 ±0.6	-0.31 ±1.0	0.268	0.02 ±0.6	-0.35 ±1.1	0.240
	TmeanSept[1]	7.4 ±0.1	7.2 ± 0.4	0.373	7.4 ±0.1	7.2 ±0.4	0.202	7.4 ±0.1	7.1 ±0.4	0.065
1965	N	12	19	----	14	17	----	16	15	----
	Elev.	3067 ±76	3162 ±83	**0.003**	3071 ±66	3171 ±87	**0.003**	3084 ±77	3170 ±87	**0.009**
	SMT	8.8 ±0.3	8.5 ±0.3	**0.004**	8.8 ±0.3	8.4 ±0.3	**0.005**	8.7 ±0.3	8.5 ±0.3	**0.024**
	LGS	160.9 ±6.8	153.2 ±7.6	**0.010**	161.1 ±6.0	152.2 ±7.6	**0.002**	159.6 ±6.9	152.5 ±7.9	**0.019**
	TmeanMay	1.6 ±1.0	0.5 ±1.2	**0.010**	1.6 ±0.9	0.4 ± 1.2	**0.002**	1.4 ±1.0	0.4 ±1.2	**0.017**
	TmeanSept	8.4 ±0.5	7.8 ±0.6	**0.010**	8.4 ±0.5	7.7 ±0.6	**0.003**	8.3 ±0.5	7.7 ±0.6	**0.021**
1978	N	17	12	----	22	7	----	23	6	----
	Elev.	3086 ±76	3190 ±80	**0.003**	3106 ±84	3203 ±83	**0.028**	3112 ±88	3194 ±86	0.090
	SMT	8.7 ±0.3	8.4 ±0.3	**0.011**	8.6 ±0.3	8.4 ±0.3	**0.037**	8.6 ±0.3	8.4 ±0.3	0.080
	LGS	159.0 ±6.9	151.1 ±7.7	**0.016**	157.6 ±7.7	149.7 ±6.7	**0.028**	157.1 ±7.9	150.3 ±7.1	0.090
	TmeanMay	1.4 ±1.0	0.2 ±1.2	**0.009**	1.1 ±1.2	0.1 ±1.0	**0.032**	1.0 ±1.2	0.2 ±1.1	0.090
	TmeanSept	8.2 ±0.5	7.6 ±0.6	**0.021**	8.1 ±0.6	7.5 ±0.5	0.055	8.1 ±0.6	7.6 ±0.6	0.142

[1] topoclimate data from Bruening (2016).

significant cooler seasonal mean temperature and shorter length of the growing season for recorder trees (Fig. 1 and Table 1). For example, in 536, despite a low number of observations (n=12), trees recording LWFR or both BR and LWFR tended ($p<0.1$) to also grow at higher elevation and to record lower seasonal mean temperatures than those not recording these anomalies. Trees recording anomalies also experience shorter and cooler growing seasons (Table 1).

3.3 Anatomy of Blue Ring and Latewood Frost Rings

Comparing the average tracheid features across anomalies (BR only, LWFR only and both BR-LWFR) using combined data from 536 and 1965 revealed few statistical differences among categories (Table 2). Among them, trees recording both BR and LWFR had earlywood tracheids with both significantly smaller lumen areas and length values than trees that recorded neither BR nor LWFR. The most significant difference however, was observed in the latewood; trees recording both BR and LWFR had latewood tracheids with significantly reduced cell wall thickness ($p<0.001$; Table 2). In both BR and LWFR, secondary walls in latewood tracheids were 37% less thick than in trees not showing the anomalies. Testing using solely the 1965 data revealed essentially the same results. Comparisons between tracheid features identified as being a constituent of a BR and/or a LWFR revealed no statistical differences between anomalies (Table 3). Both BR and LWFR were composed of about 6 tracheids on average representing about 20% of the ring width.

523 Given the absence of significant differences in BR and LWFR tracheid features, the tree rings
524 showing BR only and LWFR only were pooled with those showing both anomalies when
525 calculating the standardized tracheidograms calculated for 536 and 1965 (Fig. 7). The
526 standardized tracheidograms indicated, both in 536 and 1965, cell wall thickness was the main
527 variable differentiating tree rings showing anomalies from those not showing anomalies (Fig.
528 7cd). Starting with a CWT of about 2.5 µm, the year 536 values slightly increased to
529 approximately 3.0 µm. The recording and non-recording trees then diverged (cell 10), with the
530 tree rings presenting anomalies decreasing toward a value of 2.0 µm at the end of the growing
531 season. In 1965, a similar trend was observed with the divergence between recorder and non-
532 recorder trees occurring later in the tree ring. Compared to 536, the lumen area and lumen
533 diameter in 1965 was greater and average cell wall was more similar (Fig. 7abef). Smaller
534 differences were observed in CWT between the two years studied (Fig. 7cd). The reduced
535 lumen area and lumen width in 536 compared to 1965 also led to higher wall to cell ratio
536 observed in 536 (Fig. 7gh).

537

538

539

540

541

542

543

544 Table 2: Kruskall-Wallis one-way analysis of variance among cell features pertaining to tree
545 rings showing or not tree-ring anomalies. The data was generated from 39 bristlecone pine trees
546 and includes tree rings produced in 536 (n=12) and in 1965 (n=27). Bold number in grey box
547 indicates significant test with significant (P<0.05) Dunn-Bonferroni post-hoc test indicated by
548 different small case letters.

	Variables	No BR-LWFR	BR only	LWFR only	BR-LWFR	Pvalue
	N (536,1965)	11 (2, 9)	7 (3, 4)	3 (1, 2)	18 (6, 12)	----
EW	Tracheid No	14.81 ±8.37	18.33 ±16.04	14.22 ±2.55	21.39 ±15.60	0.635 [1]
	%	91.20 ±11.20	92.77 ±4.73	97.34 ±0.31	95.62 ±3.60	0.169 [1]
	LA (µm2)	503.61 ±114.72a	420.10 ±168.72ab	516.44 ±20.53ab	373.74 ±78.74b	**0.016** [2]
	LD(µm)	23.27 ±2.83a	20.95 ±3.54ab	25.08 ±1.96a	20.07 ±2.02b	**0.003** [2]
	CWT (µm)	2.72 ±0.38	2.74 ±0.47	2.54 ±0.80	2.41 ±0.34	0.113 [2]
	CWR (%)	0.13 ±0.03	0.14 ±0.04	0.12 ±0.5	0.13 ± 0.02	0.706 [1]
LW	Tracheid No	2.42 ±2.00	2.81 ±1.45	1.00 ±0.33	2.06 ±1.46	0.153 [1]
	%	8.80 ±11.20	7.23 ±4.73	2.66 ±0.30	4.38 ±3.60	0.169 [1]
	LA(µm2)	114.07 ±32.12	91.77 ±39.55	116.48 ±23.44	79.93 ±44.29	0.126 [1]
	LD(µm)	6.08 ±1.71	5.46 ±1.95	6.80 ±2.89	4.17 ±2.19	0.123 [1]
	CWT (µm)	2.76 ±0.43a	2.38 ±0.35ab	2.70 ±0.33ab	1.74 ±0.79b	**0.001** [2]
	CWR (%)	0.69 ±0.29	0.68 ±0.32	0.86 ±0.41	0.66 ± 0.40	0.819 [1]

549 [1] also not significant (p<0.05) using data for year 536 and 1965 separately.

550 [2] also significant (p<0.05) using data from 1965 only.

551

552

553 Table 3: Mann-Whitney U Test performed between the cell features identified as a blue ring or a
554 frost ring. The data included tree rings produced in 536 and in 1965 and for which tracheids
555 were classified as part of a blue ring or a frost ring.

Variables	Blue Ring	Frost Ring	Pvalue
N	25	21	----
Tracheid No	6.09 ±4.25	5.40 ±3.56	0.581
Total Ring (%)	20.89 ±12.71	17.69 ±7.37	0.453
Lumen area (µm2)	194.01 ±79.21	205.39 ±72.09	0.597
Lumen diameter (µm)	10.63 ±3.25	11.22 ±3.53	0.589
Cell wall thickness (µm)	2.07 ±0.41	2.00 ±0.41	0.453
Cell tracheid ratio (%)	0.38 ±0.24	0.36 ±0.21	0.843

556

557

558

559

560

561

562

563

564

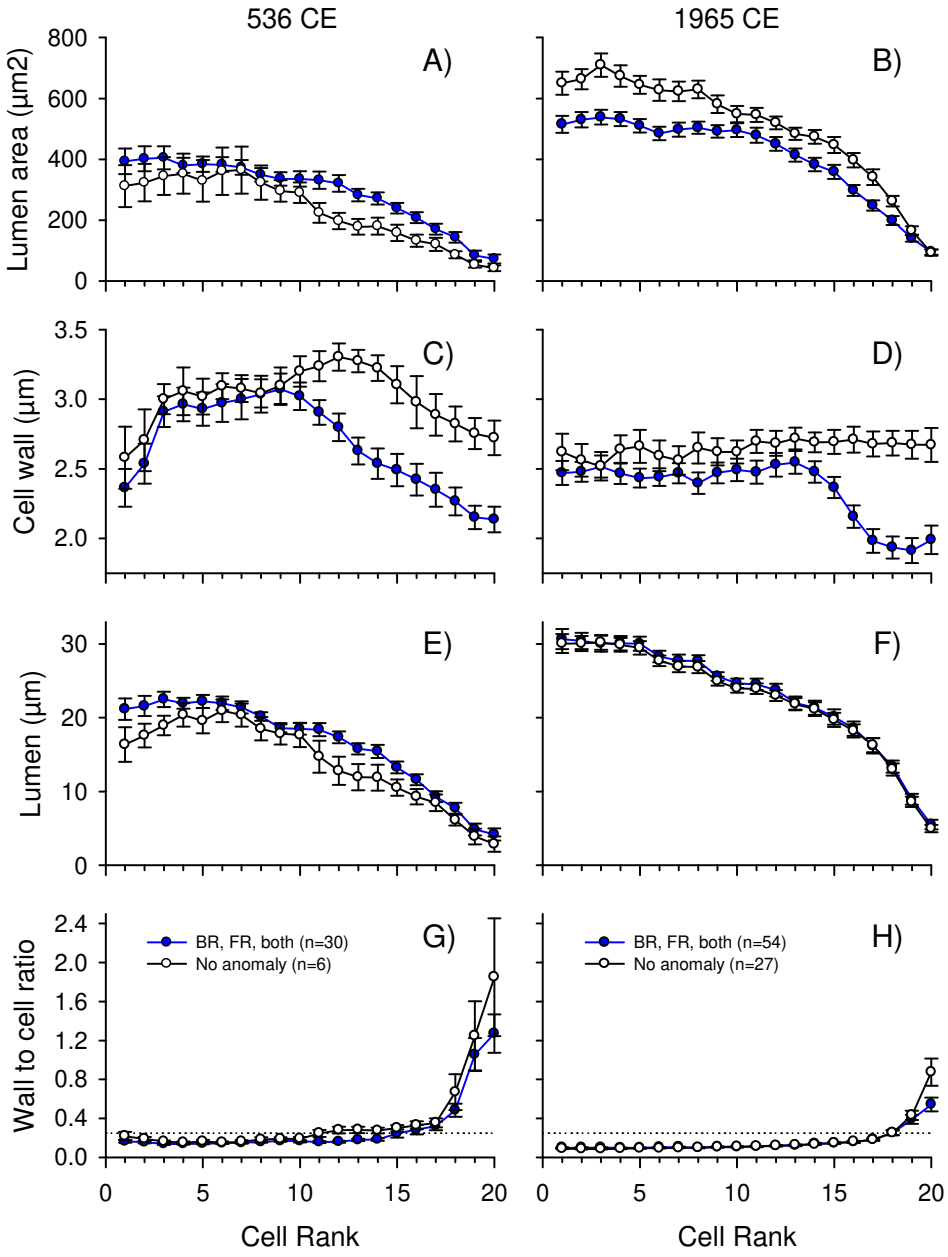

565

566 Fig. 7: Standardized tracheidograms for years 536 CE (left panel) and 1965 CE (right panel) and
567 comparing tracheid features in *Pinus longaeva* trees not recording anomalies (black lines) and
568 those recording either a blue ring, a frost ring or both (blue lines). The errors bars represent the
569 standard error of the mean. The dotted line in G and H indicates the transition from earlywood to
570 latewood tracheids (average cell wall/lumen ratio >0.25).

571 **4.0 Discussion:**

572 **4.1 Frost rings, Blue Rings and "Normal" Rings in *P. longaeva***

573 In this study, EWFR in *P. longaeva* trees were rarely observed compared to LWFR as earlier
574 noted (LaMarche and Hirschboeck 1984; Salzer and Hughes 2007). In *P. aristata*, the same point
575 was reported by others (LaMarche 1970; Brunstein 1995) with the exception of Barbosa *et al.*
576 (2019) who specifically selected sites subjected to intense cold air drainage. In numerous studies,
577 EWFR have been associated with late spring frost events following early reactivation of cambial
578 activity in years with warm springs (Stahle 1990; Montwé *et al.* 2018; Hadad *et al.* 2019; Hadad
579 *et al.* 2020). Here, maximum temperatures in May (corresponding to a Great Basin high at
580 500Mb) were positively associated with EWFR formation supporting previous findings that early
581 cambial reactivation increases the probability that trees experience and record late spring frosts.
582 Despite their low abundance, EWFR were observed more frequently in the 20th-century period
583 compared to the 6th-century period. In contrast to EWFR, LWFR have been associated with both
584 a delayed start of cambial activity and a cooler than average growing season delaying tracheid
585 maturation, thus increasing the risk of frost damages in the late growing season (LaMarche and
586 Hirschboeck 1984; Brunstein 1996; Montwé *et al.* 2018).

587

588 Latewood FR were often associated with the same individual or other nearby trees recording BR
589 in the same year. In contrast, BR were often recorded without a corresponding LWFR being
590 recorded. This indicates that cool growing seasons were not always associated with cold air
591 intrusions leading to sub-freezing temperatures in the late growing season and the formation of
592 LWFR. The lack of independence between BR and LWFR years suggests that both anomalies

593 result as a response to the same or a very similar cause: A climatic system that generates cool
594 late springs, cool summers and cool early falls. In these years, the location of a tree with regard
595 to the topographical gradient (mainly elevation) determines which *P. longaeva* trees will record a
596 BR, punctuated or not by a LWFR, i.e., if prolonged sub-freezing temperatures are encountered.
597 Our results support previous findings indicating that LWFR are associated with years with a cool
598 late spring, a cool summer and a cool early fall (LaMarche and Hirschboek 1984; Brunstein
599 1996; Barbosa *et al*. 2019). The weather conditions leading to the LWFR of 1965 have been well
600 described (LaMarche and Hirschboek 1984; Brunstein 1996; Barbosa *et al*. 2019) and will not be
601 further discussed.

602

603 Our results also indicated a lack of significant differences between tracheid features measured in
604 BR and LWFR years except that the latter clearly showed macroscopic damages resulting from
605 late growing season frosts at the time tracheids are differentiating. The frost events leading to
606 LWFR may also have prevented normal subsequent tracheid differentiation, thus accentuating
607 the presence of under-lignified tracheids. Generally, a band of under-lignified and crumpled
608 tracheids is observed as part of a FR (Glerum and Farrar 1966). In Monterey Pine (*Pinus radiata*
609 (D. Don)), Donaldson (1992) also noted poor differentiation of latewood tracheids associated
610 with FR formation. In this study, latewood secondary wall thickness in both BR and LWFR
611 years differed significantly from years with "normal" tree rings and the comparative
612 tracheidograms produced were similar to those found in LR studies (Gindl 1999; Gindl and
613 Grabner 2000). The same general departure in latewood cell wall thickness was observed when
614 compared to "normal" tree rings with no differences in lumen diameter. Unfortunately, no
615 previous BR studies to our knowledge have provided tracheid cell wall measurements.

In *P. longaeva*, BR looked very similar to the incompletely differentiated latewood tracheids described in silver fir (*Abies alba* Mill.) by Gričar *et al.* (2005; Fig.1). Their samples collected in early autumn (October 17th) presented blue-stained inner latewood wall parts which were absent in samples collected in late autumn (November 14th) which showed complete tracheid differentiation. In *P. longaeva*, BR also look similar to the unspecified BR observed in the latewood of *P. aristata* (Barbosa *et al.* 2019; Fig. 2). The BR in *P. longaeva* were also similar to some photographs of BR in *P. nigra* provided by Crivellaro *et al.* (2018; Fig. 1) and in which the under-lignified portion of the tracheid cell wall was mainly restricted to the inner portion of the wall. *Pinus longaeva* BR also appear to be more lignified than those presented in *P. nigra* (Piermattei *et al.* 2015) in which solely the cell corners were lignified indicating a premature interruption of lignification. We did not observe lignification occurring solely in the tracheid corners. Typically, tracheid lignification begins at the cell corners in the middle lamella and S1 regions, eventually spreading across the secondary wall towards the lumen after the formation of the S2 and S3 layers (Donaldson 1992).

4.2 Blue Rings and Pale Latewood (Light) Rings

Our results strongly suggest that BR and LR are representing the same irregularity, perhaps presenting a gradient in tracheid lignin content or in duration of tracheid differentiation leading to reduced secondary wall thickness. Both anomalies are associated with cooler growing season temperatures and reduced lignification of latewood tracheids. All published BR studies have identified cool growing season (early, entire or end) temperatures as the main driver for the

638 observed reduced tracheid lignification (Piermattei *et al.* 2015; Semeniuc *et al.* 2016; Crivellaro
639 *et al.* 2018; Montwé *et al.* 2018; this study). Cool growing seasons have also been associated
640 with the formation of LR in numerous coniferous species (Szeicz 1996; Gindl and Grabner 2000;
641 Gindl *et al.* 2000; Girardin *et al.* 2009; Tardif *et al.* 2011; Montwé *et al.* 2018). Light rings are
642 also characterized by reduced lignification of latewood tracheids (Gindl and Grabner 2000;
643 Grindl *et al.* 2000). Interestingly, the abnormally cool growing season conditions of 1965 that
644 caused a BR in *P. longaeva* were similar to those related to 1965 LR formation in jack pine
645 (*Pinus banksiana* Lamb.*;* Girardin *et al.* 2009, Fig. 3) in central Canada. Both LR (Brunstein
646 1995) and BR (Hughes *et al.* 2016; this study) have been reported in bristlecone pine trees.
647 Brunstein (1995) defined LR in *P. aristata* as rings with fewer latewood cells than the
648 surrounding rings leading to a narrow latewood ring. He also reported that LR and LWFR were
649 co-occurring in numerous years and he referred to various radii recording either a LR or a
650 LWFR. Similar to our findings, Brunstein (1995) reported that in 536 and in 1965 both LR and
651 LWFR were recorded (BR and LWFR in this study).

652

653 It is worth noting that LR are more difficult to detect macroscopically in coniferous species
654 producing thin latewood compared to those producing thick latewood. Among Canadian boreal
655 conifers the demarcation between LR (pale latewood) and thin latewood years is unequivocal in
656 species producing thick latewood (e.g., *P. banksiana* and *Larix laricina* ((Du Roi) K. Koch),
657 whereas identification difficulties arise with species producing thin latewood (e.g., *P. mariana*
658 and *Picea glauca* ((Moench) Voss)). In contrast to boreal pine species, *P. longaeva* trees produce
659 an extremely narrow latewood band. Like in other studies (Baas *et al.* 1986; Ziaco *et al.* 2016a)
660 tree-ring width variations in *P. longaeva* were mainly attributable to earlywood tracheids;

latewood often being composed of solely one or two cells (Mork's definition of latewood). Given that macroscopically identifying LR can present difficulties in species producing thin latewood, it may prove beneficial, in absence of more easily detectable LWFR, to assess if BR are present. Both BR and LR are proxies for cool growing season temperature with BR providing qualitative information about lignification. It still remains unclear if BR and LR can provide additional climate information compared to quantitative measurement of lignin and/or latewood density. Their observation is however less demanding in terms of costs, time and equipment. When working with species that produce little latewood it can also be challenging to distinguish LR years from thin latewood years. Future quantitative work aimed at deriving the differences between thin latewood rings and pale latewood rings (BR and LR included) in *P. longaeva* may reveal that thin latewood years and LR (BR) years provide different climate information.

4.3 Mid-6th and Late-20th Century Climate

Regional cool conditions in the 6th century are supported by the observation that our LWFR chronologies concurred with Salzer and Hughes (2007) who identified LWFR in 532, 536 and 574 in *P. longaeva* trees from various mountain ranges in the western United States. In our study, a LWFR (and BR) was also observed in 525. Salzer and Hughes (2007) also reported LWFR in 541 in the White Mountains of California. The cluster of BR recorded in 539-542 suggests that cool temperatures prevailed through the growing seasons during this extended interval. In fact, in the trees growing in the mid-6th century more annual rings recorded solely BR (without FR) in contrast to the warmer mid-20th century (Salzer *et al.* 2009). During the period centered on 1965, more EWFR were observed likely indicating the occurrence of false springs

683 and earlier onset of radial growth and potentially longer growing seasons. The positive
684 association between EWFR and warm May temperature supports these findings. Tree-ring width
685 (number of tracheids) in the 536 period was also narrower compared to the 1965 period. This
686 reduced radial growth further suggests cooler and shorter growing seasons, although it should be
687 noted that the 536 trees were growing at slightly higher elevation. The tracheid lumen area and
688 lumen diameter were also reduced in tree rings from 536 compared to 1965. Ziaco *et al.* (2014a)
689 also reported that *P. longaeva* trees growing at higher elevation produced smaller cellular
690 elements. Salzer and Hughes (2007) also observed a ring-with minimum in 536. In addition to
691 the 1941 and 1965 LWFR reported by Salzer and Hughes (2007), we also observed LWFR in
692 1964, 1978 and 1982.

693

694 The formation of LWFR in *P. longaeva* trees has been associated with outbreaks of polar air
695 during the growing season with the formation of a deep mid-tropospheric trough over the
696 western United States (LaMarche and Hirschboeck 1984; Hirschboeck et al. 1996). These
697 findings are supported by our results. The study area was significantly cooler during years
698 recording BR and/or LWFR (early, entire and late growing season) and results suggest the
699 persistence of troughs over the Great Basin region bringing cold temperatures. A recent study of
700 FR in *P. aristata* (Barbosa *et al*. 2019) also associated LWFR formation to "large-scale
701 advection of cold air masses into the west-central United States".

702

703 The presence of LWFR in high-elevation *P. longaeva* trees has been associated with
704 volcanically-forced short-term cooling events (LaMarche and Hirschboeck 1984; Hallman 2001;

705 Salzer and Hughes 2007). In this study, years with a high frequency of BR also coincided with
706 the years of volcanic eruptions. The well-studied "Dust Veil" period is known for three major
707 volcanic eruptions: 536 (unsourced eruption), 540 possibly Ilopango in El Salvador, (Sigl *et al.*
708 2015; Dull et al. 2019) or El Chichón in tropical Mexico, (Nooren *et al.* 2017), and 574 possibly
709 Rabaul in New Britain, (Sigl et al. 2015). These eruptions lead to global low irradiance and
710 associated climatic cooling with possible major societal impacts (Larsen *et al.* 2008; Sigl *et al.*
711 2015; Helama *et al.* 2018; Büntgen *et al.* 2016; Toohey *et al.* 2016). The 6th century eruptions are
712 recorded in *P. longaeva* trees as narrow tree rings with numerous BR and LWFR which, again,
713 indicates cool growing season conditions. The climate that led to the production of both BR and
714 LWFR in 1965 has been associated with lagged cooling conditions from the Mount Agung
715 eruption (Indonesia) in 1963-64 (LaMarche and Hirschboeck 1984); this was the largest and
716 most devastating eruption of the 20th century (Self and Rampino 2012). The 1978 tree-ring
717 anomalies have not been associated with any known large scale volcanic activity. As far as we
718 know, BR and LWFR in 1982 have not been previously linked to volcanic effects. However, the
719 El Chichón eruption in Mexico may be related to the *P. longaeva* anomalies we found in that
720 year. It erupted three times between March 28 and April 4, 1982 (Tilling *et al.* 1984). As
721 indicated by Nooren *et al.* (2017), the 1982 El Chichón eruption was the most disruptive in
722 modern Mexican history.

723

724 **4.4 Environmental Modulation of Radial Growth and Tree-Ring Anatomical Variations**

725 Our results indicated that slight changes in elevation (roughly 100 m) were sufficient to modulate
726 the climatic conditions leading to *P. longaeva* trees recording or not a BR or a FR. Salzer *et al.*

727 (2014) established that small changes in elevation (less than 100 m) near upper treeline can
728 modulate the response of trees to climate, shifting them from being temperature sensitive to
729 precipitation sensitive. Our BR and LWFR distributions across elevation indicate that anomalies
730 are associated with different groups of trees depending on their position along the elevation
731 gradient and on local topoclimate. For example, we observed that the elevation difference
732 between trees recording and not recording a BR, a FR, or both was generally about 90-100 m. In
733 our sample set, 536 trees grew at a higher elevation than 20th century trees, and despite fewer
734 samples (n=12), trees recording a LWFR grew at a higher elevation ($p<0.1$).

735

736 While our objective was not to assess the overall damage to trees from frost events and cool
737 summers near the altitudinal treeline, BR and lignin deficit studies suggest that reduced lignin
738 content in tracheids could lower embolism resistance and affect the safety of water transport and
739 wood mechanical properties in trees (Crivellaro *et al.* 2018; Pereira *et al.* 2018). Increased
740 porosity of the S3 layer associated with reduced lignin content could also affect the barrier
741 between the lumen and the rest of the cell wall potentially increasing the spread of pathogens in
742 trees (Donaldson 1987). The direct impact of sub-freezing temperatures (and cooler growing
743 season temperatures) at a time trees are physiologically active may affect photosynthesis
744 inducing needle loss, death of developing shoots and mortality (Lamontagne *et al.* 1998). In
745 addition to the direct physiological response, subfreezing temperature may also physically
746 damage trees. Hiratsuka and Zalasky (1993) conducted a thorough review of potential damages
747 associated with temperatures below freezing, alternation of freezing and melting, and
748 accumulation of ice glaze and snow on trees. These climatically-related damages to trees may
749 add to the complexity of the climate response in mountain environments and along short

750 elevation gradients. For dendroclimatic studies, these elements related to elevation and
751 topoclimate could influence the temporal stability of response to climate in trees growing fairly
752 closed to each other and considered growing in a uniform setting.

753

754 Results from our study further support the proposition that relatively small differences in
755 location (topographical setting) will influence the "local climate" experienced by trees which
756 could potentially lead to mixed-climate signals in mean site chronologies. We observed that the
757 impact of temperature may be observed at various elevations depending on the yearly climate,
758 thus complicating the response of *P. longaeva* trees over short altitudinal gradients (100m). Our
759 findings, in additions to those of Salzer *et al.* (2014), suggest that "signal dilution" in mountain
760 environments may occur at a much finer spatial scale than previously recognized.

761

762 **5.0 Conclusion:**

763 Our results provide a better understanding of how environmental conditions such as topography
764 and climate can modulate xylem formation in *P. longaeva* trees and the resulting tree-ring
765 anatomical features. This information can, in turn, be used to gain information about past
766 environmental conditions in which the trees grew. Our results re-emphasize the fact that the mid-
767 6th century and the mid-20th century were characterized by some years with cool growing seasons
768 leading to trees recording both BR and LWFR in their annual rings. Trees growing in the mid-6th
769 century period recorded more BR years than 20th century trees and the 6th century set of BR
770 recorded from 539-542 indicates consecutive cool growing seasons. The main tracheid feature
771 that allowed BR and LWFR to be distinguished from "normal" rings was the noticeable

772 reduction in latewood cell wall thickness; late growing season cellular damages from frost were
773 only perceptible in FR. In both anomalies this reduction and lack of lignification presumably
774 resulted from a late growing season start and a cool summer with an associated interruption of
775 tracheid differentiation (lignification) in the late growing season due to cool temperatures
776 affecting the rate and duration of cell wall deposition. All years that recorded LWFR also had at
777 least one tree recording BR in that year. In years without late growing season frosts, trees
778 recorded only BR in that year. Elevation and topoclimate were found to modulate the formation
779 of these two anomalies. More research is needed to study the impact of reduced lignification and
780 frost damages along short elevation gradients in regards to the temporal stability of the climate
781 proxy provided by tree rings. Further, our results suggested that BR (microscopic) and LR
782 (macroscopic) anomalies may originate from the same climate conditions which cause reduced
783 lignification of the latewood tracheids. The vocabulary used to describe tree-ring anomalies at
784 the macroscopic and microscopic scales may need to be re-examined and standardized to avoid
785 confusion. Lastly, macroscopic distinction between thin latewood rings and LR in tree species
786 producing narrow latewood like *P. longaeva* is challenging and may render microscopic
787 investigation of BR inevitable in climate proxy studies especially in absence of FR.

788

789 **6.0 Acknowledgement:**

790 This research was undertaken, in part, thanks to funding from the Natural Sciences and
791 Engineering Research Council of Canada (Discovery grant to J.T.), The National Science
792 Foundation's P2C2 program (1902625 and 1203749 to M.S and A.B with MKH co-PI on
793 1203749), and the Malcolm H. Wiener Foundation (M.S. collaborator). We thank Alma

794 Piermattei, Charlotte L. Pearson, Liliana Siekacz, James A. Parks, Rex Adams, Tyler J. Tran,
795 Stuart B. Weiss, and Jimmy Quenelle for their valuable contributions. The University of
796 Winnipeg and The University of Arizona also supported this research. Support for the Twentieth
797 Century Reanalysis Project version 3 dataset is provided by the U.S. Department of Energy,
798 Office of Science Biological and Environmental Research (BER), by the National Oceanic and
799 Atmospheric Administration Climate Program Office, and by the NOAA Physical Sciences
800 Laboratory. We are also grateful to the reviewers and the associate editor for providing
801 thoughtful suggestions that improved the quality of the manuscript.

802

803 **References:**

804 Baas P., Schmid R., van Heuven B.J. 1986. Wood anatomy of *Pinus longaeva* (Bristlecone Pine)
805 and the sustained length-on-age increase of its tracheids. IAWA Journal 7(3): 221-228. DOI:
806 https://doi.org/10.1163/22941932-90000988

807

808 Barbosa A.C., Stahle D.W., Burnette D.J., Torbenson M.C.A., Cook E.R., Bunkers M.J., Garfin
809 G., Villalba R. 2019. Meteorological factors associated with frost rings in Rocky Mountain
810 Bristlecone at Mt. Goliath, Colorado. Tree-Ring Research 75(2): 101-115 DOI:
811 http://dx.doi.org/10.3959/1536-1098-75.2.101

812

813 Bräuning A., De Ridder M., Zafirov, N., Garcia-González I. Dimitrov, D.P., Gärtner H. 2016.
814 Tree-ring features – indicators of extreme events impacts. IAWA Journal 2: 206-231.

815

816 Bruening J.M. 2016. Fine-scale topoclimate modeling and climatic treeline prediction of Great
817 Basin bristlecone pine (*Pinus longaeva*) in the American southwest. Master's thesis
818 Environmental Science, Western Washington University, Bellingham, WA.

819

820 Bruening J.M., Tran T.J., Bunn A.G., Weiss S.B., Salzer M.W. 2017. Fine-scale modeling of
821 bristlecone pine treeline position in the Great Basin, USA. Environmental Research Letters
822 12(1): 14008.

823

824 Bruening J.M., Bunn A.G., Salzer M.W. 2018. A climate–driven tree line position model in the
825 White Mountains of California over the past six millennia. Journal of Biogeography 45(5): 1067-
826 1076.

827

828 Brunstein F.C. 1995. Bristlecone pine frost-ring and light-ring chronologies, from 569 BC to AD
829 1993, Colorado. U.S. Geological Survey, Open-File Report 95-63, US Geological Survey, 25 pp.

830

831 Brunstein F.C. 1996. Climatic significance of the bristlecone pine latewood frost-ring record at
832 Almagre Mountain, Colorado, U.S.A. Arctic and Alpine Research 28: 65-76.

833

834 Bunn A.G., Hughes M.K., Salzer M.W. 2011. Topographically modified tree-ring chronologies
835 as a potential means to improve paleoclimate inference. Climatic Change 8: 627-634.

836

837 Bunn A.G., Salzer M.W., Anchukaitis K.J., Bruening J.M., Hughes M.K. 2018. Spatiotemporal
838 variability in the climate growth response of high elevation bristlecone pine in the White
839 Mountains of California. Geophysical Research Letters 45: 13312-13321.
840 https://doi.org/10.1029/2018GL080981

841

842 Büntgen U., Myglan V.S., Ljungqvist F.C., McCormick M., Cosmo N.D., Sigl M., Jungclaus J.,
843 Wagner S., Krusic P.J., Esper J., Kaplan J.O., de Vaan M.A.C., Luterbacher J., Wacker L., Tegel
844 W., Kirdyanov A.V. 2016. Cooling and societal change during the late antique little ice age from
845 536 to around 660 AD. Nature Geoscience 9: 231-236, 10.1038/ngeo2652

846

847 Churakova (Sidorova) O.V., Bryukhanova M.V., Saurer M., Boettger T., Naurzbaev M.M.,
848 Myglan V.S., Vaganov E.A., Hughes M.K., Siegwolf R.T.W. 2014. A cluster of stratospheric
849 volcanic eruptions in the AD 530s recorded in Siberian tree rings. Global Planetary Change 122,
850 140-150. https://doi.org/10.1016/j.gloplacha.2014.08.015

851

852 Crivellaro A., Reverenna M., Ruffinatto F., Urbinati C., Piermattei A. 2018. The anatomy of
853 “blue ring” in the wood of *Pinus nigra*. Les/Wood67(2): 21-28. DOI:
854 https://doi.org/10.26614/les-wood.2018.v67n02a02

Daly C., Halbleib M., Smith J.I., Gibson W. P., Doggett M.K., Taylor G.H., Curtis J., Pasteris P.O. 2008. Physiographically sensitive mapping of climatological temperature and precipitation across the conterminous United States. International Journal of Climatology 28(15): 2031-2064. https://doi.org/10.1002/joc.1688

D'Arrigo R., Frank D., Jacoby G., Pederson N. 2001. Spatial response to major volcanic events in or about AD 536, 934 and 1258: frost rings and other dendrochronological evidence from Mongolia and northern Siberia. Climatic Change 49: 239-246.

De Micco V., Campelo F., De Luis M., Bräuning A., Grabner M., Battipaglia G., Cherubini P. 2016. Intra-annual density fluctuations in tree rings: how, when, where, and why? IAWA Journal 37: 232-259.

DeSoto L., de la Cruz M., Font P. 2011. Intra-annual pattern of tracheid size in the Mediterranean *Juniperus thuriferaas* indicator for seasonal water stress. Canadian Journal of Forest Research 41:1280–1294. DOI: 10.1139/x11-045

Donaldson L.A. 1987. S3 lignin concentration in radiata pine tracheids. Wood Science and Technology 21: 227-234.

Donaldson L.A. 1992. Lignin distribution during latewood formation in *Pinus radiate* D. Don. IAWA Journal 13(4): 381-387. DOI: https://doi.org/10.1163/22941932-90001291

Dull R.A., Southon J.R., Kutterolf S., Anchukaitis K.J., Freundt A., Wahl D.B., Sheets P., Amaroli P., Hernandez W., Wiemann M.C., Oppenheimer C. 2019. Radiocarbon and geologic evidence reveal Ilopango volcano as source of the colossal 'mystery' eruption of 539/40 CE. Quaternary Science Review 222(15): 105855. https://doi.org/10.1016/j.quascirev.2019.07.037

Gärtner H., Banzer L., Schneider L., Schweingruber F.H., Bast A. 2015. Preparing microsections of entire (dry) conifer increment cores for wood anatomical time-series analyses. Dendrochronologia 34: 19-23.

888 Gindl W. 1999. Climatic significance of light rings in Timberline spruce, *Picea abies*, Austrian
889 Alps. Arctic, Antarctic, and Alpine Research 31(3): 242-246.
890 DOI:10.1080/15230430.1999.12003304

891

892 Gindl W., Grabner M. 2000. Characteristics of spruce [*Picea abies* (L.) Karst.] latewood formed
893 under abnormally low temperatures. Holzforschung 54: 9-11.

894

895 Gindl W., Grabner M., Wimmer R. 2000. The influence of temperature on latewood lignin
896 content in treeline Norway spruce compared with maximum density and ring width. Trees 14:
897 409-414.

898

899 Girardin M., Tardif J.C., Epp B., Conciatori F. 2009. Frequency of cool summers in interior
900 North America over the past 3 centuries. Geophysical Research Letters 36: L07705. DOI:
901 10.1029/ 2009GL037242.

902

903 Glerum C., Farrar J.L. 1966. Frost ring formation in the stems of some coniferous species.
904 Canadian Journal of Botany 44: 879-886.

905

906 Gričar J., Čufar K., Oven P., Schmitt U. 2005. Differentiation of terminal latewood tracheids in
907 silver fir trees during autumn. Annals of Botany 95(6): 959–965. doi:10.1093/aob/mci112.

908

909 Gurskaya M.A., Shiyatov S.G. 2006. Distribution of frost injuries in the wood of conifers.
910 Russian Journal of Ecology 37(1): 7-12. DOI: 10.1134/S1067413606010024

911

912 Gurskaya M.A. 2014. Temperature conditions of the formation of frost damages in conifer trees
913 in the high latitudes of western Siberia. Biology Bulletin 41: 187-196.

914

915 Hadad M.A., Arco Molina J., Roig Juñent F.A., Amoroso M.M., Müller G., Araneo D., Tardif
916 J.C. 2019. Frost records in tree rings linked to atmospheric circulation in northern Patagonia.
917 Palaeogeography, Palaeoclimatology, Palaeoecology 524: 201-211.

918

919 Hadad M.A., Tardif J.C., Conciatori F., Waito J., Westwood A. 2020. Climate and atmospheric
920 circulation related to frost-ring formation in *Picea mariana* trees from the Boreal Plains, interior

North America. Weather and Climate Extremes 29: 100264.
https://doi.org/10.1016/j.wace.2020.100264.

Haldon J. 2016. Cooling and societal change. Nature Geoscience 9: 191-192.

Hallman C.L. 2001. Spatial relationships in frost damaged high elevation pines and links to major volcanic eruptions. MSc. Thesis, The University of Arizona.

Hantemirov R.M., Gorlanova L.A., Shiyatov S.G. 2004. Extreme temperature events in summer in northwest Siberia since AD 742 inferred from tree rings. Palaeogeography, Palaeoclimatology, Palaeoecology 209: 155-164.

Helama S., Jones P.D., Briffa K.R. 2017. Dark Ages Cold Period: A literature review and directions for future research. The Holocene 27(10): 1600-1606.

Helama S., Arppe L., Uusitalo J., Holopainen J., Makela H.M., Makinen H., Mielikainen K., Nojd P., Sutinen R., Taavitsainen J.P., Timonen M., Oinonen M. 2018. Volcanic dust veils from sixth century tree-ring isotopes linked to reduced irradiance, primary production and human health. Nature Scientific Reports 8(1339): DOI: 10.1038/s41598-018-19760-w

Helama S., Saranpää P., Pearson C.L., Arppe L., Holopainen J., Mäkinen, H., Mielikäinen K., Nöjd P., Sutinen R., Taavitsainen J.-P., Timonen M., Uusitalo J., Oinonen M. 2019. Frost rings in 1627 BC and AD 536 in subfossil pinewood from Finnish Lapland. Quaternary Science Review 204: 208-215.

Hiratsuka Y., Zalasky H. 1993. Frost and other climate-related damage of forest trees in the prairie provinces. Forestry Canada, Northwest Region, Northern Forestry Centre, Edmonton, Alberta. Information Report NOR-X-331.

Hirschboeck K.K., Ni F., Wood M.L., Woodhouse C.A. 1996. Synoptic dendroclimatology: Overview and prospectus. In Tree Rings, Environment, and Humanity, edited by Dean J.S., D. M. Meko D.M., Swetnam T.W., pp. 205–223. Radiocarbon, Tucson, AZ.

954 Hoffer M., Tardif J.C. 2009. False rings in jack pine and black spruce trees from eastern
955 Manitoba as indicators of dry summers. Canadian Journal of Forest Research 39: 1722-1736.

956

957 Hughes M.K., Piermattei, A., Salzer M.W., Gärtner H. 2016. Blue rings in multi-century
958 bristlecone pine from near upper tree limit in California and Nevada, USA. AmeriDendro 2016,
959 Third American Dendrochronology Conference, March 28 - April 1, 2016, Mendoza, Argentina.

960

961 Körner C. 2012. Alpine treelines: Functional ecology of the global high elevation tree limits.
962 Berlin: Springer Science & Business Media. https://doi.org/10.1007/978-3-0348-0396-0

963

964 LaMarche V.C. 1970. Frost-damage rings in subalpine conifers and their application to tree-ring
965 dating problems. In: Smith J.H.G. and Worral J. (eds.), Tree-ring analysis with special reference
966 to Northwest America. Fac. Forest Bull. 7: 99–100. University of British Columbia, Vancouver.

967

968 LaMarche V.C. Jr., Hirschboeck K.K. 1984. Frost rings in trees as records of major volcanic
969 eruption. Nature 307: 121-126.

970

971 Lamontagne M., Margolis H., Bigras F. 199. Photosynthesis of black spruce, jack pine, and
972 trembling aspen after artificially induced frost during the growing season. Canadian Journal of
973 Forest Research 28: 1-12.

974

975 Larsen L.B., Vinther B.M., Briffa K.R., Melvin T.M., Clausen H.B., Jones P.D., Siggaard-
976 Andersen M.-L., Hammer C.U., Eronen M., Grudd H., Gunnarson B.E., Hantemirov R.M.,
977 Naurzbaev M.M., Nicolussi K. 2008. New ice core evidence for a volcanic cause of the A.D. 536
978 dust veil, Geophysical Research Letters 35, L04708, doi:10.1029/2007GL032450.

979

980 Matisons R., Gärtner H., Elferts D., Kārkliņa A., Adamovičsa A., Jansonsa A. 2019. Occurrence
981 of 'blue' and 'frost' rings reveal frost sensitivity of eastern Baltic provenances of Scots pine.
982 Forest Ecology and Management 457: 117729. https://doi.org/10.1016/j.foreco.2019.117729

983

984 Moreland J. 2018. AD536 – Back to nature? Acta Archaeologica 89(1): 91-111.
985 https://doi.org/10.1111/j.1600-0390.2018.12194.x

986

987 Nooren K., Hoek W. Z., Van der Plicht H., Sigl M., Van Bergen M. J., Galop D., Torrescano-
988 Valle N., Islebe G., Huizinga A., Winkels T., Middelkoop H. 2017. Explosive eruption of El
989 Chichón volcano (Mexico) disrupted 6th century Maya civilization and contributed to global
990 cooling. Geology 45(2): 175-178. Doi:10.1130/G38739.1

991

992 Montwé D., Isaac-Renton M., Hamann A., Spiecker H. 2018. Cold adaptation recorded in tree
993 rings highlights risks associated with climate change and assisted migration. Nature
994 Communication 9(1): 1574. doi: 10.1038/s41467-018-04039-5.

995

996 Newfield T.P. 2018. The climate downturn of 536-550. Pp. 447-493 In Pfister C., Mauelshagen
997 F. (eds.), The Palgrave Handbook of Climate History, White S., Palgrave, London.
998 https://doi.org/10.1057/978-1-137-43020-5_32

999

1000 Novak K., De Luis M., Gričar J., Prislan P., Merela M., Smith K.T., Čufar K. 2016. Missing and
1001 dark rings associated with drought in *Pinus halepensis*. IAWA Journal 37: 260-274.

1002

1003 Park Y.-I., Dallaire G., Morin H. 2006. A method for multiple intra-ring demarcation of
1004 coniferous trees. Annals of Forest Science 63(1): 9-14.

1005

1006 Pereira L., Domingues-Junio A.P., Jansen S., Choat B., Mazzafera P. 2018. Is embolism
1007 resistance in plant xylem associated with quantity and characteristics of lignin? Trees 32: 349-
1008 358. https://doi.org/10.1007/s00468-017-1574-y

1009

1010 Piermattei A., Crivellaro A., Carrer M., Urbinati C. 2015. The "blue ring": anatomy and
1011 formation hypothesis of a new tree-ring anomaly in conifers. Trees 29(2): 613-620.
1012 doi:10.1007/s00468-014-1107-x

1013

1014 R Core Team 2013. R: A language and environment for statistical computing. R Foundation for
1015 Statistical Computing, Vienna, Austria. URL http://www.R-project.org/.

1016

1017 Salzer M.W., Hughes M.K. 2007. Bristlecone pine trees and volcanic eruptions over the last
1018 5000 yr. Quaternary Research 67: 57-68.

1019

1020 Salzer M.W., Hughes M.K., Bunn A.G., Kipfmueller K.F. 2009. Recent unprecedented tree-ring growth
1021 in bristlecone pine at the highest elevations and possible causes. Proceedings of the National Academy of
1022 Sciences 106(48):20348-20353, doi:10.1073/pnas.0903029106.
1023

1024 Salzer M.W., Bunn A.G., Graham N.E., Hughes M.K. 2013. Five millennia of paleotemperature
1025 from tree-rings in the Great Basin, USA. Climate Dynamics 42: 1517-1526.
1026 http://dx.doi.org/10.1007/s00382-013-1911-9

1027

1028 Salzer M.W., Larson E.R., Bunn A.G., Hughes M.K. 2014. Changing climate response in near-
1029 treeline bristlecone pine with elevation and aspect. Environmental Research Letters 9: 114007

1030

1031 Schneider L., Gärtner H. 2013. The advantage of using a starch based non-Newtonian fluid to
1032 prepare micro sections. Dendrochronologia 31: 175-178.

1033

1034 Schweingruber F.H. 2007. Wood Structure and Environment. Springer Science & Business
1035 Media, Heidelberg. 279 pp.

1036

1037 Self S., Rampino M.R. 2012. The 1963–1964 eruption of Agung volcano (Bali, Indonesia).
1038 Bulletin of Volcanology 74, 1521–1536. https://doi.org/10.1007/s00445-012-0615-z

1039

1040 Semeniuc A.I., Sidor C.G., Popa I. 2016. Scots pine tree ring structure modifications and relation
1041 with climate. Eurasian Journal of Forest Science 4(2): 1-7.

1042

1043 Szeicz J.M. 1996. White spruce light rings in northwestern Canada. Arctic and Alpine Research
1044 28: 184-189.

1045

1046 Sigl M., Winstrup M., McConnell J.R., Welten K.C., Plunkett G., Ludlow F., Büntgen U., Caffee
1047 M., Chellman N., Dahl-Jensen D., Fischer H., Kipfstuhl S., Kostick C., Maselli O.J., Mekhaldi
1048 F., Mulvaney R., Muscheler R., Pasteris D.R., Pilcher J.R., Salzer M., Schüpbach S., Steffensen
1049 J.P., Vinther B.M., Woodruff T.E. 2015. Timing and global climate forcing of volcanic eruptions
1050 during the past 2500 years. Nature 523: 543-549. doi:10.1038/nature14565

1051

1052 Slivinski L.C., Compo G.P., Whitaker J.S., Sardeshmukh P.D., Giese B.S., McColl C. et al. 2019
1053 Towards a more reliable historical re-analysis: Improvements for version 3 of the twentieth

century re-analysis system. Quarterly Journal of the Royal Meteorological Society 145(724): 2876-2908. https://doi.org/10.1002/qj.3598

Stahle D.W. 1990. The tree-ring record of false spring in the southcentral USA. Ph.D. thesis, Arizona State University, Temper, Arizona, 272 pages.

Tardif J.C., Conciatori F. 2015. Microscopic Examination of Wood: Sample Preparation and Techniques for Light Microscopy. In Plant Microtechniques and Protocols, Chapter: 22, Publisher: Springer International Publishing, Editors: Yeung E.C.T., Stasolla C., Sumner M.J., Huang B.Q. (Eds, pp.373-416) DOI: 10.1007/978-3-319-19944-3

Tardif J.C., Girardin M.P, Conciatori F. 2011. Light rings as bioindicators of climate change in interior North America. Global Planetary Change 79: 134-144.

Tilling R. I., Rubin M., Sigurdsson H., Carey S., Duffield W.A. Rose W.I. 1984. Holocene eruptive activity of El Chichón volcano, Chiapas, Mexico. Science 224: 747-749.

Toohey M., Krüger K., Sigl M., Stordal F., Svensen H. 2016. Climatic and societal impacts of a volcanic double event at the dawn of the Middle Ages. Climatic Change 136(3): 401-412.

Tran T.J., Bruening J.M., Bunn A.G., Salzer M.W., Weiss S.B. 2017. Cluster analysis and topoclimate modeling to examine bristlecone pine tree-ring growth signals in the Great Basin, USA. Environmental Research Letters 12: 014007.

Trouet V., van Oldenborgh G.J. 2013. KNMI Climate Explorer: A web-based research tool for high-resolution paleoclimatology. Tree-Ring Research 69(1): 3-13.

Vaganov E.A. 1990. The tracheidogram method in tree-ring analysis and its application. In: Cook E.R., Kairiukstis L.A., eds. Methods of Dendrochronology – Applications in the Environmental Sciences. Dordrecht, The Netherlands/Boston, USA/London, UK: Kluwer Academic Publishers, 63-76.

1086 Vaganov E.A., Hugues M.K., Shashkin A.V. 2006. Growth Dynamics of Conifer Tree Rings:
1087 Images of Past and Future Environments. Springer, New York, USA.

1088

1089 Waito J., Conciatori F., Tardif J.C. 2013. Frost rings and white earlywood rings in *Picea*
1090 *mariana* trees from the boreal plains, Central Canada. IAWA Journal 34: 71-87.

1091

1092 Wimmer R. 2002. Wood anatomical features in tree-rings as indicators of environmental change.
1093 Dendrochronologia 20: 21-36.

1094

1095 Wimmer R., Strumia G., Holawe F. 2000. Use of false rings in Austrian pine to reconstruct early
1096 growing season precipitation. Canadian Journal of Forest Research 30: 1691-1697.

1097

1098 Ziaco E., Biondi F., Rossi S Deslauriers A. 2014a. Climatic influences on wood anatomy and
1099 tree-ring features of Great Basin conifers at a new mountain observatory. Applied Plant Science
1100 2(10): 1400054. doi: 10.3732/apps.1400054.

1101

1102 Ziaco E., Biondi F., Rossi S., Deslauriers A. 2014b. Intra-annual wood anatomical features of
1103 high-elevation conifers in the Great Basin, USA. Dendrochronologia 32: 303-312. http://
1104 dx.doi.org/10.1016/j.dendro.2014.07.006

1105

1106 Ziaco E., Biondi F.B., Heinrich I. 2016a. Wood cellular dendroclimatology: Testing new proxies
1107 in great basin bristlecone pine. Frontiers in Plant Science 1(7): 1602. DOI:
1108 10.3389/fpls.2016.01602

1109

1110 Ziaco E., Biondi F., Rossi S., Deslauriers A. 2016b. Environmental drivers of cambial phenology
1111 in Great Basin bristlecone pine. Tree Physiology 36(7): 818-831. doi: 10.1093/treephys/tpw006